AFIT/GEO/ENG/92D-02

OPTICAL HAAR WAVELET TRANSFORMS USING COMPUTER GENERATED HOLOGRAPHY

THESIS

Peter G. Block
Captain, USAF

AFIT/GEO/ENG/92D-02

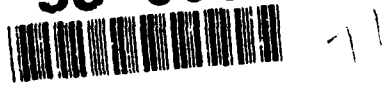

AFIT/GEO/ENG/92D-02

OPTICAL HAAR WAVELET TRANSFORMS USING COMPUTER GENERATED HOLOGRAPHY

THESIS

Presented to the Faculty of the School of Engineering
of the Air Force Institute of Technology
Air University
In Partial Fulfillment of the
Requirements for the Degree of
Master of Science in Electrical Engineering

Peter G. Block, B.S.E.E.
Captain, USAF

17 December, 1992

Preface

I now understand why many individuals do not choose to perform experimental research for a Master's thesis. It takes a great deal of time and effort, and if there's a chance something can go wrong, it will. Despite the problems encountered, it has also been a truly rewarding experience.

I wish to thank my committee members, Dr. Dennis Ruck, and Dr. Mark Oxley for their support throughout this research project. I would also like to thank Dr. Byron Welsh. Without his help, I would still be staring at computer generated holograms and wondering if they were really encoding the desired functions. Thanks also go to Dr. Steven Rogers, whose help, guidance, and extreme patience made the entire research effort enjoyable. I would be remiss if I didn't also thank Mr. Bill Tropp and Mr. Don Smith of the Cooperative Electronics Lab who taught me more than I ever cared to know about photoreduction using the dekagon camera system.

I thank my parents for providing me with the desire to learn and the gifts to make it possible. Lastly and most importantly, I thank my wife, Elizabeth, who was my inspiration throughout this effort. I couldn't have made it without her support.

Peter G. Block

Table of Contents

List of Figures

Abstract

This research introduces an optical implementation of the continuous wavelet transform to filter images. The wavelet transform is modeled as a correlation process and is implemented with a Vander Lugt correlator. The orthonormal basis set used is composed of two one-dimensional Haar functions and a two-dimensional Haar function. Each wavelet, as well as its first two dyadic scalings, is implemented with computer generated holography. The Interferogram method, which represents a function only in terms of its phase, is used to encode the wavelet functions.

The results are imaged onto a CCD array and captured using a framegrabber. The optical results are compared to digital simulation. The results show that an optical implementation of the continuous wavelet transform was performed and that the results compared favorably to digital simulation.

OPTICAL HAAR WAVELET TRANSFORMS USING COMPUTER GENERATED HOLOGRAPHY

I. Introduction

The Air Force has expended considerable effort attempting to develop an automatic machine-based pattern recognition system. The machine based system has particular advantages as part of a smart weapon system. Applications range from recognizing a tank in a cluttered scene to identifying terrorists as they enter an airport. An autonomous system requires no direct cueing by a human operator, and has clear advantages in circumstances where a human being may not perform well or where human life is at risk. This research discusses a subsystem of a machine-based pattern recognition system called an image segmentor.

Traditionally, pattern recognition is broken down into three areas: segmentation, feature extraction, and classification. Segmentation of potential targets from cluttered scenes is the first step before classification can begin (22). Image segmentation is simply finding potential targets in a cluttered scene (21). Feature extraction picks the critical attributes of the segmented image such as the length-to-width ratio or the bright spot intensity and passes that information to the classification subsystem. Finally, the classification subsystem compares the feature extraction data to features of previously classified or known objects (21). The result is the identification of the image as a tank, truck, or terrorist. Once identified, the machine-based system will either initiate action against the segmented object, or continue to search for potential targets.

Numerous methods have been proposed for the segmentation of digital imagery with some success (5, 6, 9, 18, 20, 22, 23); however, the problem is far from solved.

Significant research has also been performed in the medical field (15). A method known as computed tomography is currently used to allow physicians to diagnose clinical abnormalities from the display of a three-dimensional organ image (15). This technique segments the organ of interest from the rest of the body and then a computer transforms the two dimensional image captured by a camera into a three-dimensional object (15). This technique works well for an stationary organ but it will not work when the object of interest is a moving target such as a tank.

In addition to the tremendous computational resources required by the above methods, the time required to perform the segmentation is unpractical for a real-time system to be used on a smart weapon. An optical image segmentation system, if realizable, would improve system performance. With an optical system, the thousands of computations required by a digital computer can be performed in the amount of time it takes the light to travel from one end of the system to the other.

1.1 Problem Statement

This research introduces an optical implementation of the continuous wavelet transform (implemented with computer generated holography) for filtering images.

1.2 Approach

The block diagram of the image segmentation system used is shown in Figure 1. This outlines the various steps utilized in obtaining the filtered image. Several different types of mathematical functions, called wavelets, are tested in the system. Each wavelet is encoded in a computer generated hologram (CGH) and then correlated optically with a cluttered scene containing an object of interest. This system yields a filtered version of the input image in the correlation plane. The resolution of the resultant filtered image is analyzed as a function of wavelet type and dilation. Ideally, the results obtained from this research can be passed to a neural network based image segmentor to complete the segmentation process (20).

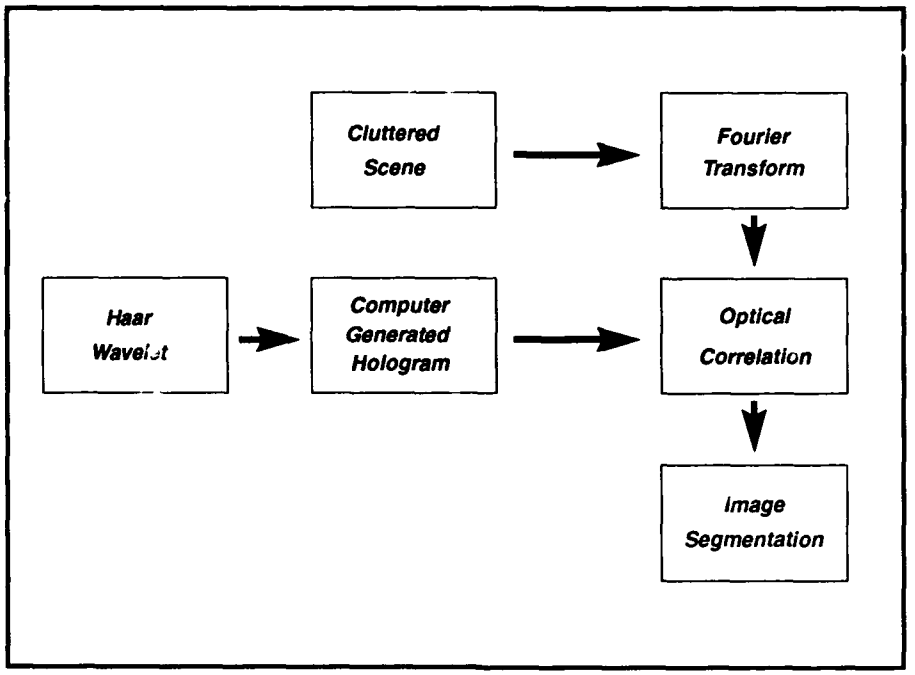

Figure 1. Optical segmentation approach

1.3 Scope

This research is a continuation of that conducted by Capt Pinski. The major goal is to improve upon the resolution of the filtered images obtained in his research (18). It also implements all three wavelet basis functions that make up the complete orthonormal basis set rather than just the two basis functions used by Capt Pinski. The primary objective of this research is to optically implement the continuous wavelet transform utilizing computer generated holography. The filtered images were captured and stored on a digital computer. The optically segmented images are compared to results obtained using a digital simulation of the optical system.

1.4 Outline of Thesis

Chapter II provides the necessary background on the different techniques employed in computer generated holography as well as an in-depth discussion of the

binary interferogram technique used in this research. Additionally, a brief survey of related work is presented. Chapter III discusses in detail the applicable theory of optical wavelet-based image segmentation . The optical correlation system is validated by comparing to digital simulation. In Chapter IV, wavelets and the continuous wavelet transform are introduced. The results obtained during this research effort are also presented along with a detailed analysis. Specifically, filter performance is discussed along with its dependencies on both: type of wavelet and its corresponding dilation. Chapter V presents a comparison of results to those obtained by previous work. It also presents conclusions reached and provides recommendations for future research. Lastly, detailed appendices are provided to describe exactly how the CGHs were encoded and then processed in order to be used in the optical system.

II. Holography and Computer Generated Holograms

2.1 Vander Lugt Filtering

In order to understand how CGHs are encoded and used, an introduction to holography and its applications is required. In photography, light from a scene is recorded on film in terms of the intensity(magnitude) of the electro-magnetic light waves squared. The phase of the light waves is not recorded. In holography however, it is possible to record both the magnitude as well as the phase of the light waves. In 1963, A. B. Vander Lugt developed a process to record both the magnitude and phase of an object optically(10). The optical set-up proposed by Vander Lugt interfered an object of the form $A(x,y)e^{j\phi(x,y)}$ with a tilted reference wave represented by $Re^{j\pi\alpha x}$. The resulting intensity is given by the transmittance function, t(x,y), given below(13):

$$\mathrm{t}(x,y) \;=\; \mathrm{R}^2 + \mathrm{A}^2(x,y) + 2\mathrm{RA}(x,y)\cos[2\pi\alpha x - \phi(x,y)]. \qquad (1)$$

The expression is both real and nonnegative. It can also be recorded with conventional film. The system used to record this intensity is called a Vander Lugt Filter and is shown in Figure 2.

In Figure 2, S indicates the location of the point source that is collimated by lens L1. The collimated source illuminates the input at P1 located a focal length away from lens L2. This lens then Fourier transforms the input at the film plane where it interferes with a reference beam approaching at an angle α determined by the prism, P. The amplitude and phase information are recorded as amplitude and phase modulations of a high frequency carrier introduced by the reference beam (10). Therefore, the light from the object optically interferes with the reference beam, and the resultant interference pattern is recorded on the film. When a slide made from

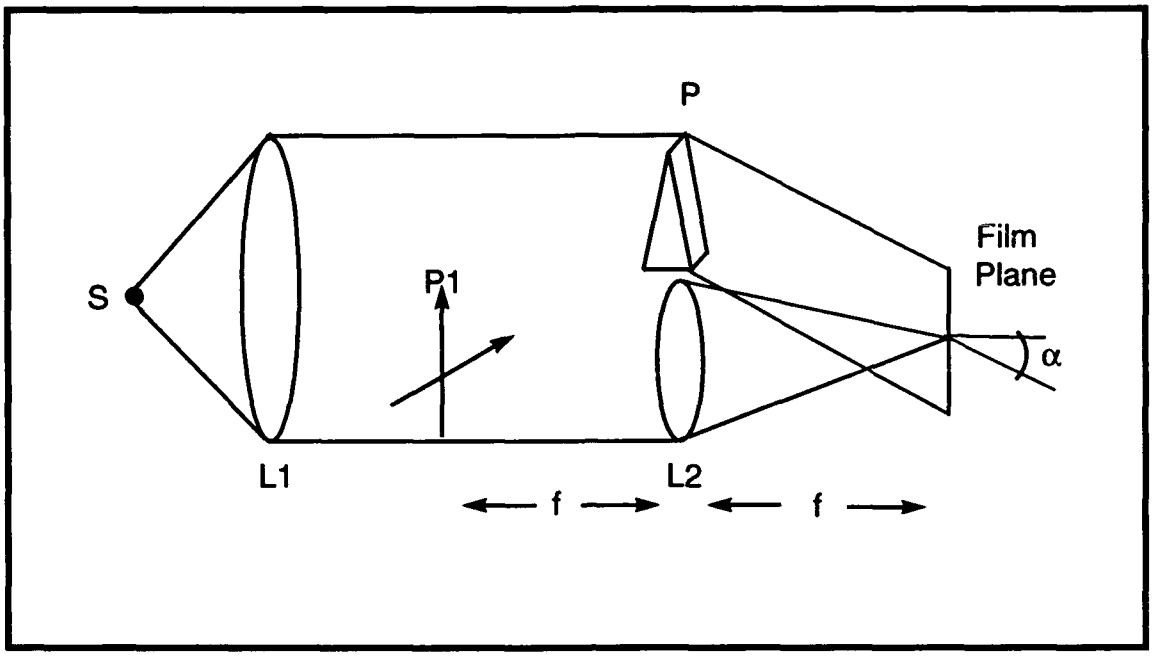

Figure 2. Vander Lugt Filter (10)

the film is illuminated in the system of Figure 3, the original input image is located in the back focal plane of lens L2 off-axis at the angle α.

Unlike conventional holograms, computer generated holograms(CGHs) or computer holograms are produced as a graphical output from a digital computer(13). The main advantage to this holographic method is that it enables the encoding of analytical expressions which previously were unable to be created using conventional methods. In the case of a CGH, the object function, $A(x,y)e^{j\phi(x,y)}$, is known. Once a carrier frequency α is introduced, the complex object function can be encoded using a modified version of equation 1 given by(13):

$$\mathrm{t}(x,y) \;=\; .5(1+\mathrm{A}(x,y)\cos[2\pi\alpha x-\phi(x,y)]). \qquad (2)$$

There are several different methods available for converting the desired wavefront into a real, non-negative function encoded in the CGH. Some methods encode

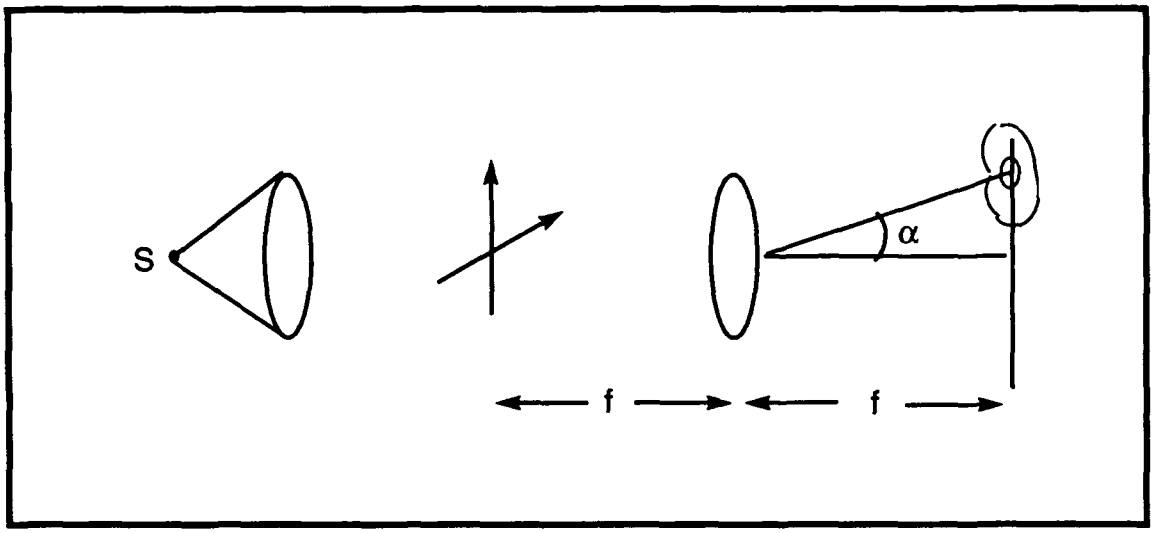

Figure 3. System to illuminate Vander Lugt Filter (10)

magnitude and phase while others encode only the phase. The interferogram method, which encodes only the phase of the desired function, was chosen to carry out this research. The remainder of this chapter describes the interferogram CGH, why it was chosen, and the techniques required to encode it.

2.2 The Interferogram

The interferogram method of recording a CGH encodes only the phase of the expression and ignores the amplitude. Since often the majority of the information describing a function is contained in the phase, ignoring the amplitude information should have minimal effect on the results(13). This also simplifies the encoding of the function. The amplitude information is ignored by setting A(x,y) equal to one in Equation 2 and yields:

$$t(x,y) = .5(1+\cos[2\pi\alpha x - \phi(x,y)]). \quad (3)$$

Since the cosine function oscillates between one and negative one, the transmittance function of Equation 3 oscillates between zero and one. Maximum values of the transmittance function occur when the argument of the cosine function is a multiple of 2π, or:

$$2\pi\alpha x - \phi(x,y) \;=\; 2\pi n_k. \tag{4}$$

In Equation 4, n_k is a list of integers ranging from zero up to the number of maxima in the transmittance function. The pairs of (x,y) values which satisfy Equation 4 correspond to the locations of the maximum values of the transmittance function and also define the locations of the interference fringes in the hologram (13). The contrast of the fringes improve if only the fringe peaks are recorded(12). Therefore, a binary device such as a laser printer can be used to plot the interference fringes. The resulting hologram is called a computer generated interferogram. The plot is then photo-reduced onto a glass slide using the system discussed in Appendix A.

Two types of CGH system architectures were considered for this research. The first type encodes the phase of the desired object function. When the complex wavefront encoded in a CGH is created by the superposition of an object beam with a reference beam, the object is reconstructed with a plane wave (12). The system required for this system architecture is shown in Figure 4. The second type encodes the phase of the two-dimensional Fourier transform of the desired object function. This type of CGH is reconstructed using the system shown in Figure 5. In this system the CGH is also illuminated with a plane wave. The lens Fourier transforms the CGH to yield the reconstructed object function. The system architecture shown in Figure 5 is the one chosen for this research. For reasons to be discussed in the next chapter, this method is best suited for the optical correlation system used in this research.

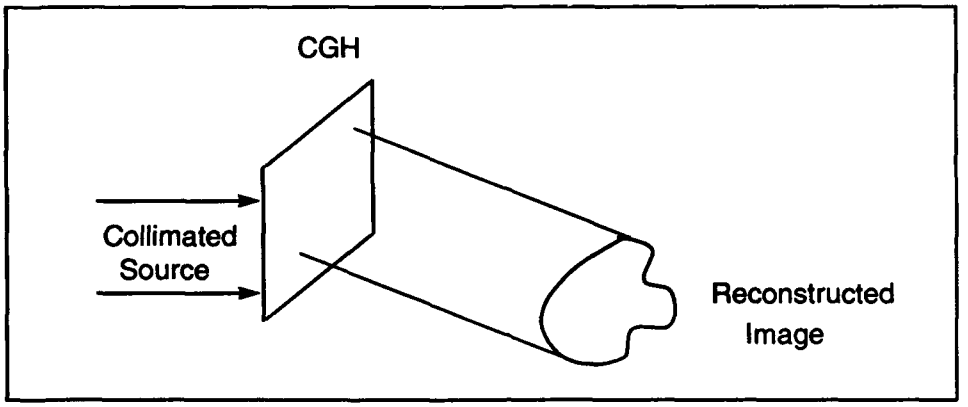

Figure 4. Image reconstruction from CGH encoded with phase of object image (12)

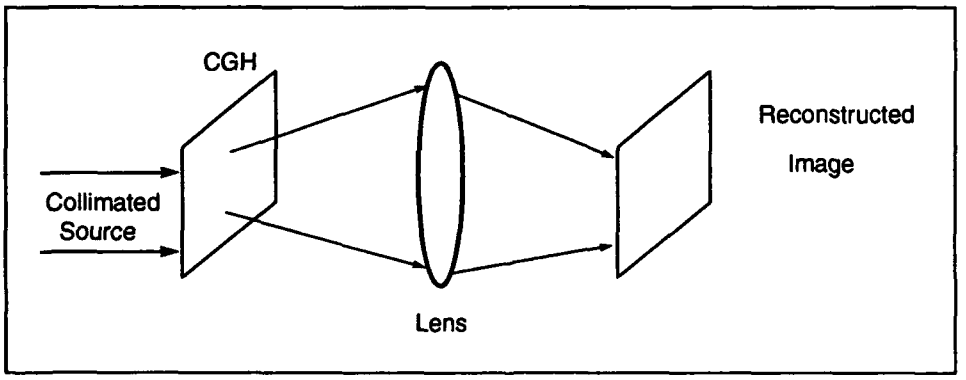

Figure 5. Image reconstruction from CGH encoded with 2-D Fourier transform of object image (12)

The hologram consists of fringes, or grating lines, allowing the desired wavefront to be produced by diffracting illuminating light through the grating(12). Since the carrier frequency, α, represents a reference beam, illumination of the CGH using the system of Figure 6 will result in the reconstruction of conjugate images at angles $\pm\alpha$, $\pm 2\alpha$, etc. depending on the diffraction efficiency of the CGH. It is therefore extremely important to choose α correctly to prevent any overlap of these multiple orders.

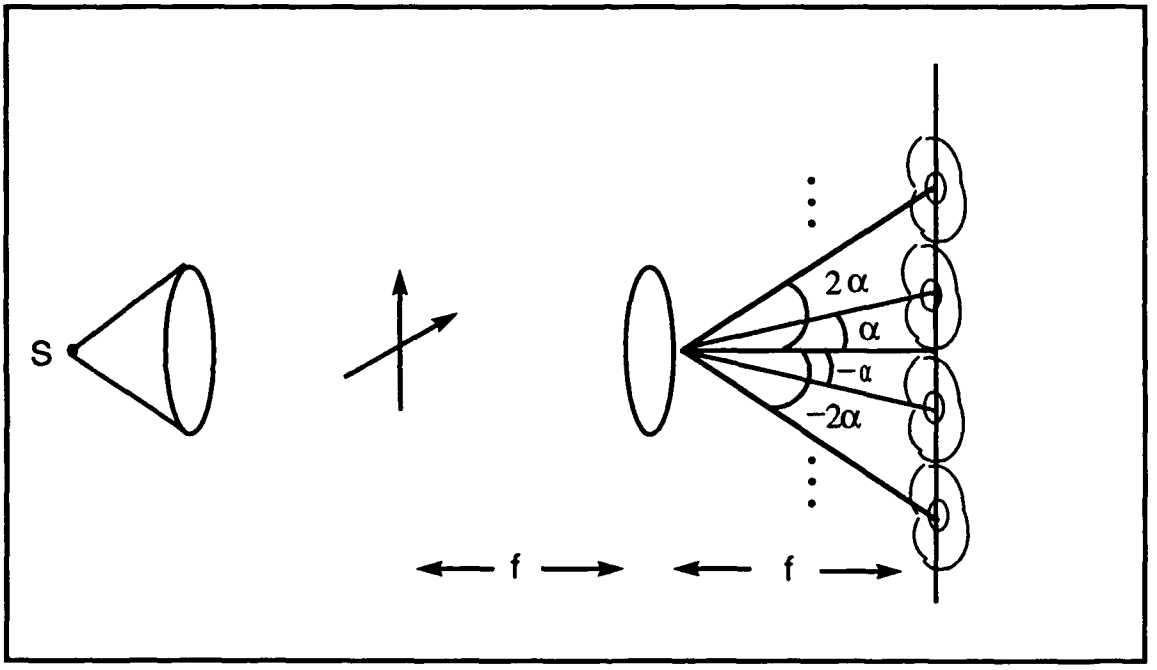

Figure 6. System to illuminate CGH (13)

The most important consideration after the type of CGH and the system architecture to be used is the proper selection of the carrier frequency. In order to separate the first order diffracted wave from the second order wave, a sufficiently high carrier frequency must be chosen. Since the multiple orders are located along the x-axis (as defined by Equation 3), it is necessary to consider only the spatial frequencies of the input object along the x-direction. The relationship between α

and U_{max}, the maximum spatial frequency in the x-direction, is given by (13):

$$\alpha > 2U_{max} \tag{5}$$

For an input object that has resolution of X pixels in the x-direction, the highest spatial frequency, U_{max}, possible is determined by:

$$U_{max} = X/(input\ dimension\ in\ x-direction) \tag{6}$$

Therefore, for an input image consisting of 128 x 128 pixels and size of 10 mm x 10mm, $\alpha > 2(128/10) = 25.6\ lines/mm = 12.8\ cycles/mm$. Once α has been chosen, the CGH can be created.

This chapter provided the basic information required to understand conventional holography as well as computer generated holography. The Interferogram method, described by Equation 3, was discussed in detail. The system architecture for this research, as well as the system required to illuminate a CGH were also described. Lastly, the importance of the carrier frequency, α was discussed in addition to the method used to correctly choose it. The next chapter introduces image segmentation and describes how it can be performed optically. Additionally, a method to validate the entire system from CGH encoding to the optical implementation is proposed and tested.

III. Methodology

3.1 Image Segmentation

The first task required to solve the pattern recognition problem is to extract the object of importance (the potential target) from the given scene. Once segmented, the important features of the image can be extracted and sent to the pattern classifier to identify the image. Each subsystem depends on the information passed by its predecessor to perform its task.

Although each subsystem is optimized individually, in reality the pattern recognition system is only as good as its worst subsystem. In other words, the pattern classifier relies on the feature extractor to not only extract the best features, but extract them accurately. In order for the feature extractor to perform well, it requires a high quality or high resolution segmented image. Therefore, the image segmentation subsystem is the foundation of any good pattern recognition system (19). A good pattern recognition system is one that not only correctly identifies targets, but identifies them quickly as well.

Until recently, research to improve pattern recognition systems was limited to improving algorithms based in digital computers. To improve the speed of the overall system, pinski proposed an optical image segmentation scheme utilizing a Magneto-optic Spatial Light Modulator (18). Although the speed of the segmentation was improved significantly, the resolution of the segmented image was less than predicted. The poor resolution was caused by the limited resolution of the spatial light modulator (18). Therefore, if the resolution can be improved, an optical segmentation scheme is clearly the best choice for an image segmentation subsystem.

3.2 Optical Implementation

One way to filter an image is to perform a cross correlation operation. If a cluttered scene is correlated with a function that highlights edges, a segmented image is obtained (22). The cross correlation of a cluttered scene, denoted by f(x,y), with an edge-detection function, denoted by g(x,y), is defined by (8):

$$f(x,y) \star g(x,y) \;=\; \int_{-\infty}^{\infty} \int_{-\infty}^{\infty} f(\alpha,\beta)\, g(\alpha - x,\, \beta - y)\, d\alpha\, d\beta \qquad (7)$$

A cross correlation can also be obtained by taking the Fourier transform of the product of each function's Fourier transform. If $\mathcal{F}$ is defined as the Fourier operator, then the Fourier transform operation can be written as:

$$\mathcal{F}\,[\, f(x,y)\,] \;=\; F(\xi,\eta) \qquad (8)$$

Equation 7 is rewritten as:

$$f(x,y) \star g(x,y) \;=\; \mathcal{F}\,[F(\xi,\eta) \cdot G(-\xi,-\eta)] \qquad (9)$$

The operation described by Equation 9 lends itself extremely well to an optical implementation.

The system shown in Figure 7 optically implements the cross correlation operation as described in Equation 9. Lens L1 collimates the point source, S. The cluttered scene is placed at plane, P1. Lens L2 Fourier transforms the scene at plane P2 where it is multiplied by the CGH of the edge-detection function. The CGH is inserted at P2 in a flipped configuration (about the horizontal and vertical axes) to satisfy Equation 9. Lens L3 Fourier transforms the product and the cross correlation is located at the output plane, P3. Once again, the method in which the CGH is encoded causes the multiple cross correlations shown.

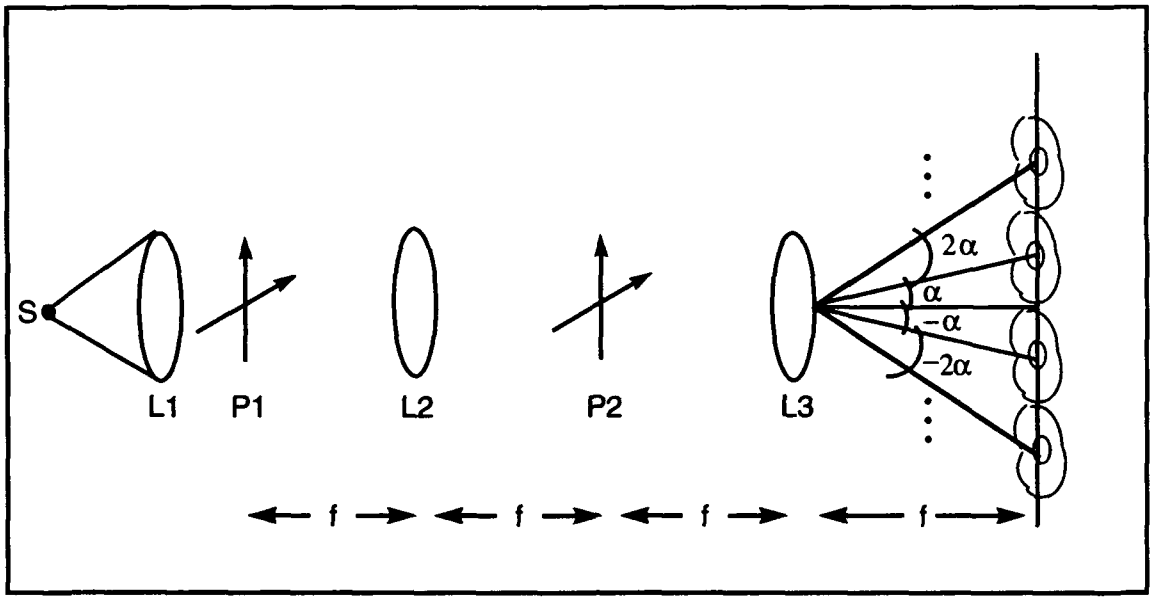

Figure 7. Optical system to perform cross correlation (10)

3.3 Method Verification

In order to ensure the CGH encoding methods, its software implementation, as well as the optical system all function as predicted, a total system validation is required. If a function is used as the input image and it is also encoded in the CGH, the optical system of Figure 7 performs an auto-correlation of the function with itself. To properly validate the system operation, the optical results obtained are compared to those obtained by digital simulation.

The two-dimensional rectangle function is chosen to perform the validation and is defined below:

$$\text{rect}(x,y) = \begin{cases} 1 & \text{if} \quad -.5 \leq x \leq .5 \quad \text{and} \quad -.5 \leq y \leq .5 \\ 0 & \text{otherwise.} \end{cases} \tag{10}$$

A three-dimensional plot of the rectangle function is shown in Figure 8. To implement this function in the optical system of Figure 7, a two-dimensional square

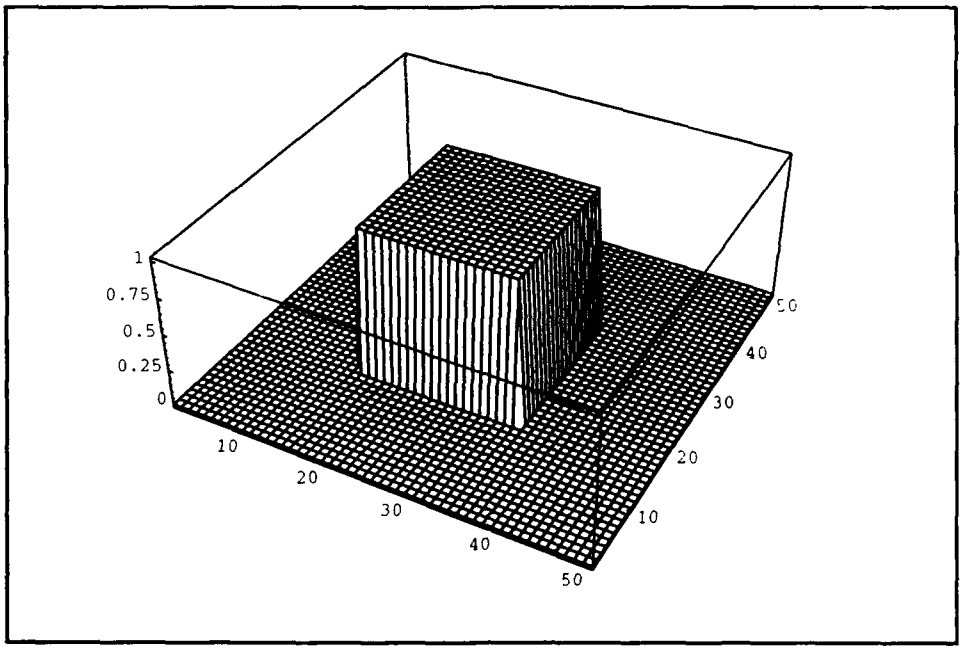

Figure 8. 3-D plot of rectangle function

aperture is placed at plane,P1. It is necessary to take the Fourier transform of the rectangle function to encode the CGH. The two-dimensional Fourier transform of the rectangle function is given below:

$$\mathcal{F}\,[\,\mathrm{rect}(x,y)\,] \;=\; \mathrm{sinc}(\xi,\eta). \tag{11}$$

A function is completely described by its absolute value, or magnitude, and its corresponding phase. The three-dimensional plot of the magnitude of the sinc function is shown in Figure 9. Its phase function is shown in Figure 10. Note that the phase function is discrete, having values of either zero or π. The phase is zero valued over intervals where the sinc and the magnitude of the sinc are identical in value and sign. The phase function has a value of π over the intervals where the sinc is negative. It is the phase of the Fourier transform of the desired function that is encoded in the Interferogram CGH. The Interferogram was created using the software and methods

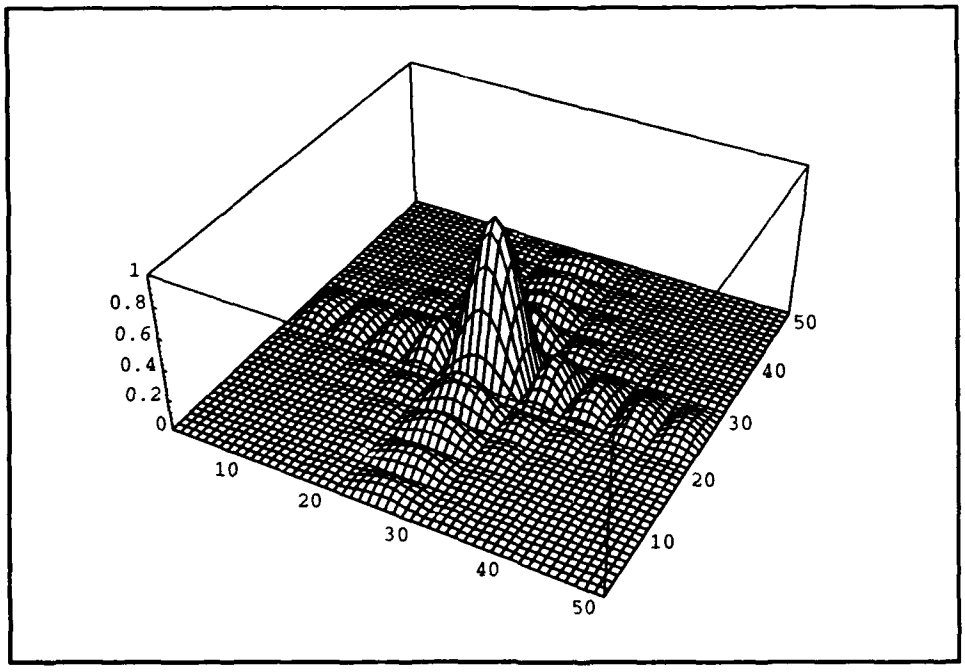

Figure 9. 3-D plot of the magnitude of the sinc function

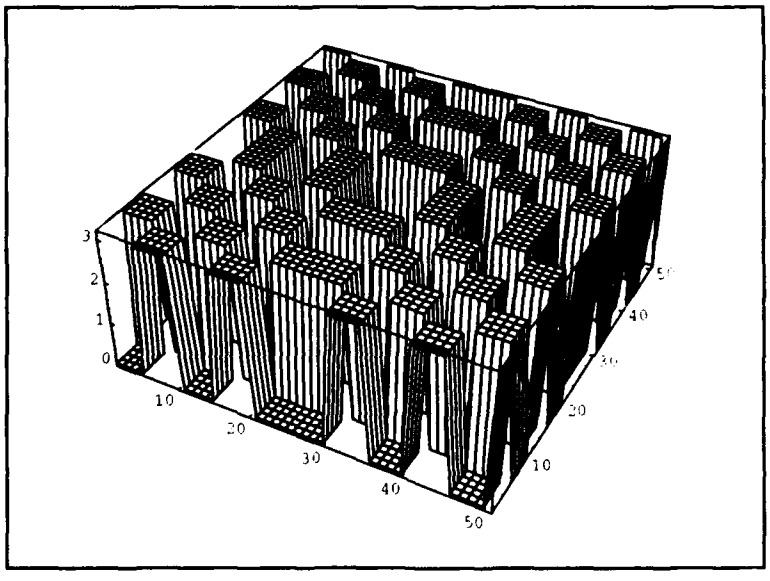

Figure 10. 3-D phase plot of the magnitude of the sinc function

outlined in the appendices. The plot of the Interferogram is shown in Figure 11. To validate the encoding operation, the CGH was made and placed in the optical

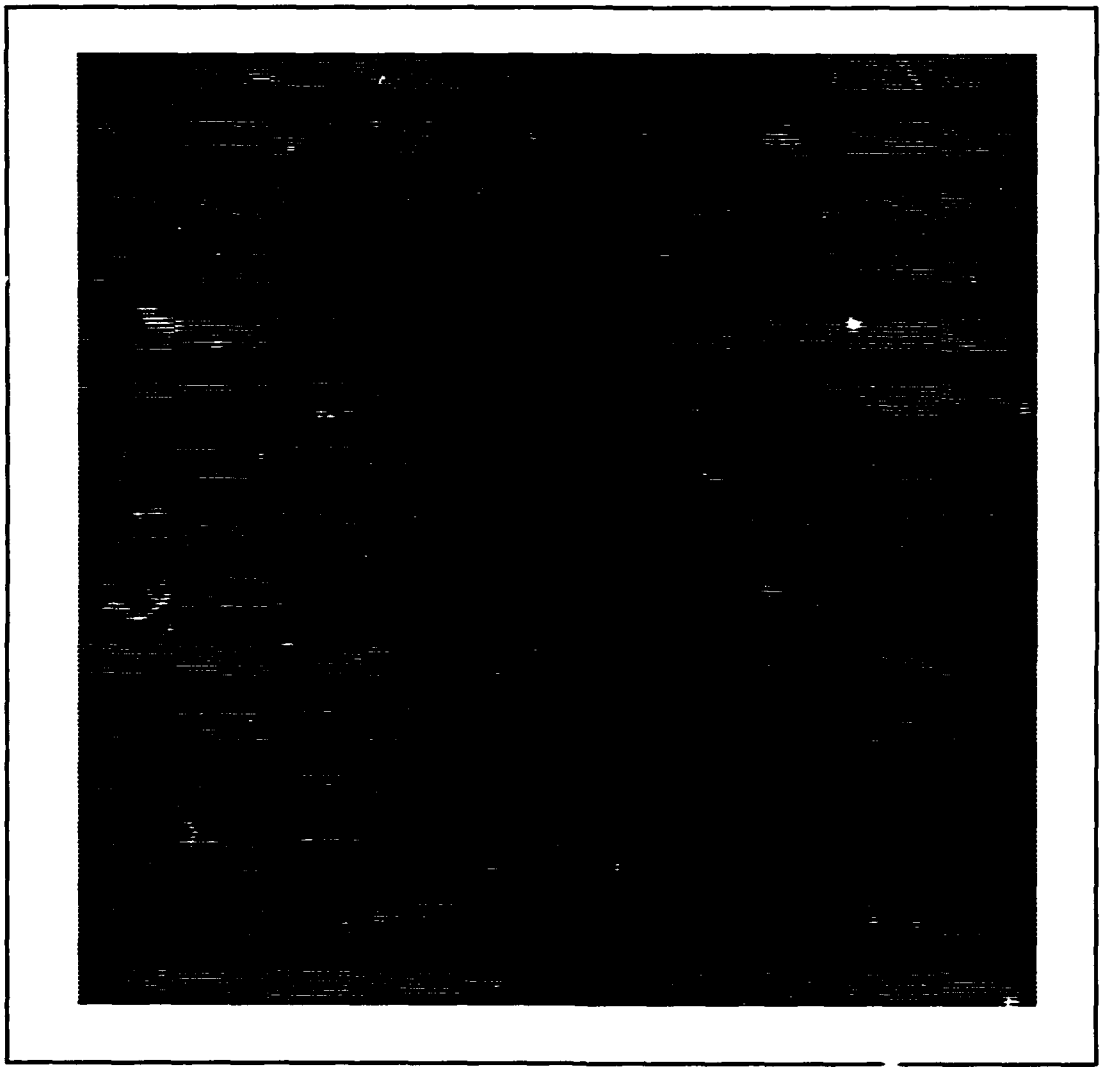

Figure 11. Plot of interferogram of two-dimensional rectangle function

set-up shown previously in Figure 5. When the CGH is illuminated, the lens Fourier transforms the function encoded and the result is located in the back focal plane of the lens. The result obtained was captured with a CCD camera, stored, and is shown in Figure 12. It is important to note that the CGH encodes only the phase

of the sinc. The amplitude is not encoded. For this reason, the Fourier transform is not a perfect rect as shown in Figure 8. Since it is difficult to predict what the Fourier transform will be, a digital simulation was performed. The digital simulation is shown in Figure 13. The digital simulation compares very well with the optical result. Careful inspection of Figure 13 shows four main peaks corresponding to the four corners of the rectangle function as well as multiple secondary peaks located outside of the main peaks. When the optical result was obtained, only the main peaks were captured and stored.

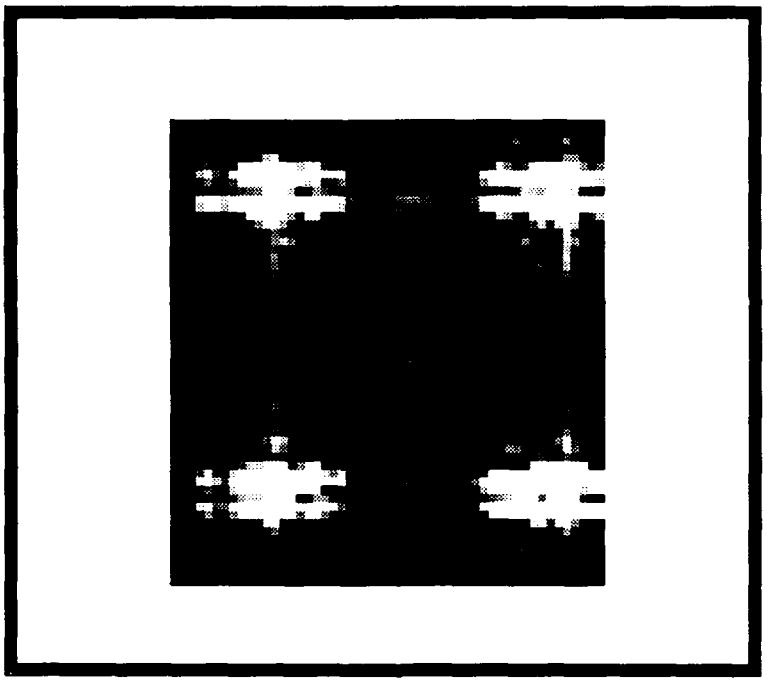

Figure 12. Optical Fourier transform of phase of sinc function encoded in CGH

Once the CGH encoding method and software were validated, the optical correlation system was tested. Again, the square aperture was placed in the input plane, P1 and the CGH was placed in plane, P2. The result was captured and stored and is shown in Figure 14. The digital simulation result is shown in Figure 15. It is extremely difficult to compare the optical result with the digital simulation because

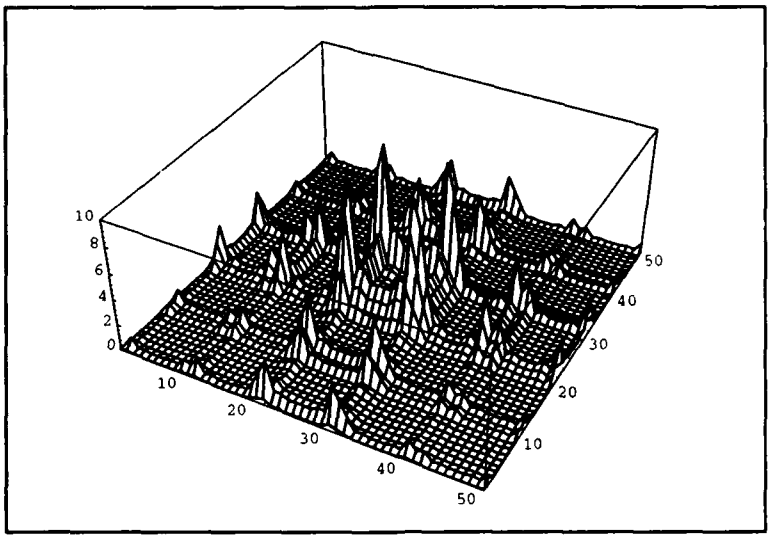

Figure 13. Digital simulation of Fourier transform of phase of sinc function encoded in Interferogram CGH

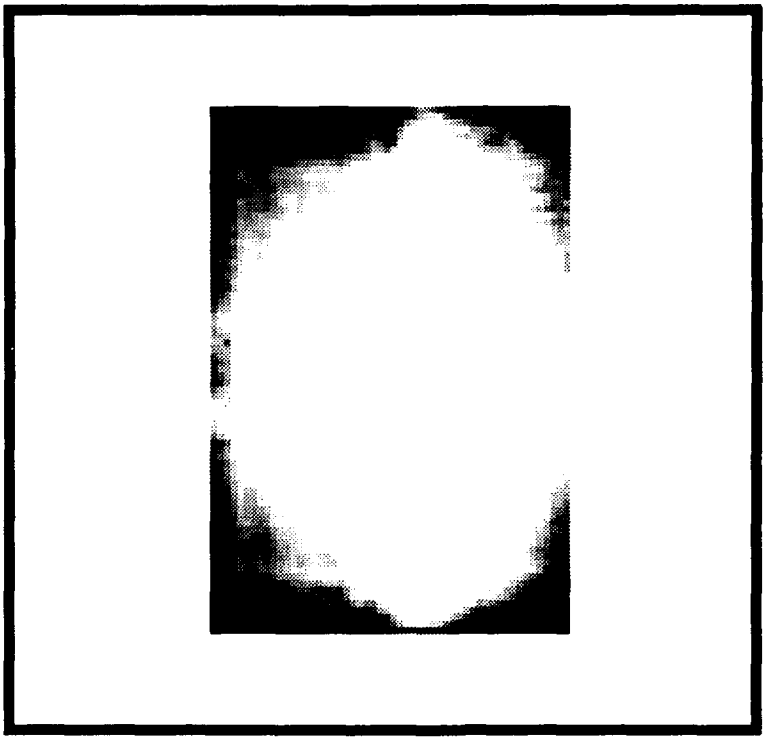

Figure 14. Optical result of the auto-correlation of the rectangle function with itself

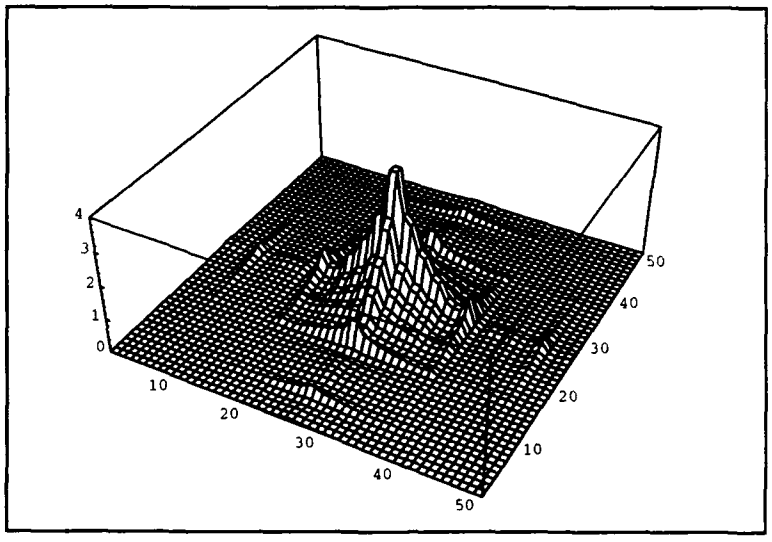

Figure 15. Digital simulation of the auto-correlation of the rectangle function with itself

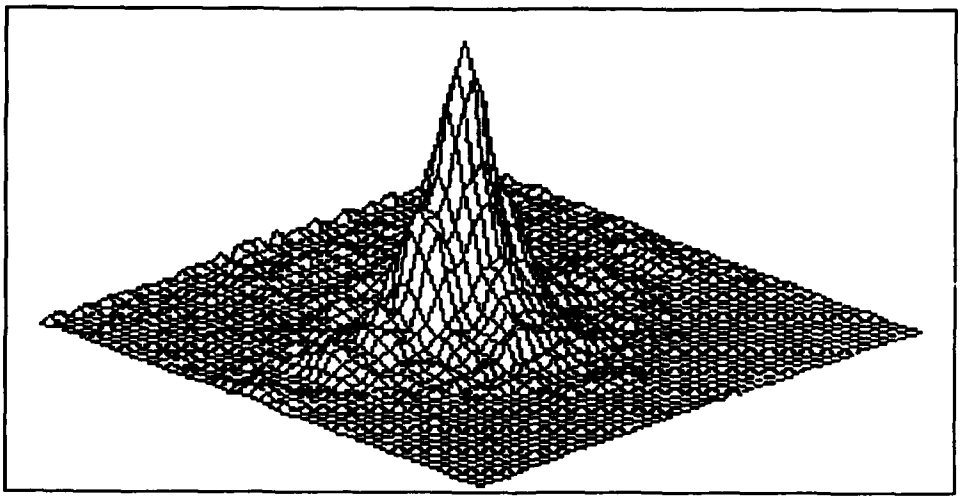

Figure 16. Optical result of the auto-correlation of the rectangle function with itself using Beam Code Software

the center peak is so dominant that it washes out the rest of image. For this reason, a laser beam analysis tool called Beam Code Software(4) was obtained from the Engineering Physics Department at AFIT to properly analyze the result. Although the primary purpose of the Beam Code Software is to analyze laser beam modes and spot size, it works well for this application. The tool uses a radiation detector that has a much larger dynamic range than the CCD camera. This allows the entire image to be captured without having the bright central intensity peak washing out any of the remaining signal. The detector was placed in the output plane and the results were stored, processed, and displayed with a conventional CRT display. The result obtained using the Beam Code Software was displayed as a three-dimensional graphic to allow easy comparison to the digital simulation. This result is shown in Figure 16 . The result is almost identical to the digital simulation.

Now that the total system is validated, the next phase of the research can begin. The next chapter gives a brief introduction to wavelets, the continuous wavelet transform, and describes the methods used to perform the optical image segmentation.

IV. Results and Discussions

Image segmentation has been tried using several different image processing techniques with varied results (15, 20, 22). This research implements a method known as wavelet analysis (20). The wavelet transform can be described by a Fourier filtering operation, where the inherent filtering operation of the wavelet transform passes certain frequencies while attenuating others. The type of wavelet chosen determines which frequencies are passed and which are filtered. It is also possible to adjust the filtering characteristics by varying a parameter of the wavelet called the dilation. The remainder of this chapter describes the wavelet transform and discusses how it is implemented in the optical correlator system presented in Chapter 2.

4.1 Wavelet Analysis

The Fourier transform gives no information about where specific frequencies are located in the original signal. The wavelet transform, on the other hand, provides both frequency and location information with respect to the input image or signal. A wavelet transform decomposes an image into scaled, translated, and dilated versions of a transform kernel referred to as a mother wavelet (6). Due to the kernel's translational properties, the wavelet transform can be characterized as a correlation process (6). As stated in the previous chapter, correlation processes are well suited for optical implementation.

The filters in a wavelet analysis are derived from shifted and dilated versions of the mother wavelet. The mother wavelet acts as a window in the temporal or spatial domain, allowing certain frequencies to be passed and attenuating others. The form of the two-dimensional mother wavelet, ψ_{abcd} , is given by the following expression(6):

$$\psi_{abcd} = \frac{1}{\sqrt{ad}} \psi \left(\frac{x-b}{a}, \frac{y-c}{d} \right). \tag{12}$$

In this expression, the variables a and d denote the dilation or width of the wavelet, which varies the size of the window used in the filtering process (20). The variables b and c denote the translation or location of the wavelet along the x and y axes. Since the correlation process will automatically perform all possible translations of the wavelet, the translation variables will be set to zero and ignored in the remainder of this discussion. Therefore, the mother wavelet will always be located at the origin. The correlation process cannot produce the energy normalization factor, $\frac{1}{\sqrt{ab}}$, but this does not affect the validity of the wavelet transform as discussed in the article by Burns et al (6). This reduces Equation 12 to:

$$\psi_{ad} = \psi\left(\frac{x}{a}, \frac{y}{d}\right). \tag{13}$$

In Equation 13, all positive values of a and d provide for all possible dilations of the mother wavelet which make up the basis set, ψ_{ad} (20). This basis set provides broad windows for large dilations corresponding to narrow bandwidth filters that yield a coarse resolution analysis of a scene, and small dilations corresponding to wide bandwidth filters that capture high spatial frequencies. The result provides details unable to be detected with the larger dilation. For this reason, wavelet analysis is sometimes called multiresolution analysis.

The continuous wavelet transform of an image, i(x,y) is given by:

$$[W_\psi i](a,b,c,d) = \int\int_{-\infty}^{+\infty} i(x,y)\frac{1}{\sqrt{ad}}\psi\left(\frac{x-b}{a}, \frac{y-c}{d}\right)dxdy. \tag{14}$$

For a more detailed discussion of wavelet transforms, read the article by Burns et al (6).

The wavelet transform can be described as the projection of the image onto a basis set made up of all shifts of a scaling function at a fixed dilation. By choosing discrete dilations properly, a discrete multiresolution analysis is performed by decomposing an image into its basis set of images, thus representing the image by its

wavelet transform coefficients. The image can then be reconstructed by combining the coefficients without performing every possible dilation. Just as an image can be approximated by a subset of its Fourier coefficients, it can also be approximated by a set of discrete wavelet transform coefficients. The next section describes how multiple dilations of a scaling function can be used to perform a multiresolution analysis on a two-dimensional image.

4.2 Multiresolution Analysis

Multiresolution analysis represents an image as a series of projections, each of which approximates the original image at different levels of resolution (20). The levels of resolution correspond to different dilations of a scaling function which can be combined to produce an orthonormal wavelet basis set. For two-dimensional images, the orthonormal basis set is composed of three wavelet basis functions, $\Psi^1(x,y), \Psi^2(x,y), \Psi^3(x,y)$, which are constructed from two, one-dimensional scaling functions, $\phi(x)$ and $\phi(y)$, and the mother wavelet, $\psi(x,y)$. The scaling functions can be thought of as passband controllers or filters in the frequency domain. Each successively larger scaling function and mother wavelet combination filters a successively narrower band of frequencies. The three wavelet basis functions are given below (16):

$$\begin{aligned} \Psi^1(x,y) &= \phi(x)\psi(y) \\ \Psi^2(x,y) &= \phi(y)\psi(x) \\ \Psi^3(x,y) &= \psi(x)\psi(y) \end{aligned} \tag{15}$$

It is common practice to take scaling functions at dilations that are powers of two (also known as the dyadic scaling functions) to obtain an orthonormal basis set for a multiresolution analysis(16). This research used three dilations of the scaling functions. The first dilation does not alter the mother wavelet; the second doubles

the width of the mother wavelet, and the third quadruples the width of the mother wavelet. This will provide the successive filtering operation discussed earlier.

4.3 The Haar Wavelet

The wavelet chosen to perform this research is the Haar wavelet. To form the orthonormal basis set, $\Psi^1(x,y), \Psi^2(x,y), \Psi^3(x,y)$, three variations of the Haar wavelet are necessary. The orthonormal basis set consists of two one-dimensional Haar wavelets and the two-dimensional Haar wavelet. The expression for the first, one-dimensional wavelet, Haar(x) is given below:

$$\text{Haar}(x) = \begin{cases} 1 & \text{if } -.5 \leq x < 0 \\ -1 & \text{if } 0 \leq x < .5 \\ 0 & \text{otherwise} \end{cases} \tag{16}$$

This function will highlight vertical edges when correlated with an image using the optical correlator of Figure 7. The three dimensional plot of the function is shown in Figure 17. In order to encode this function in a CGH, it is first necessary to

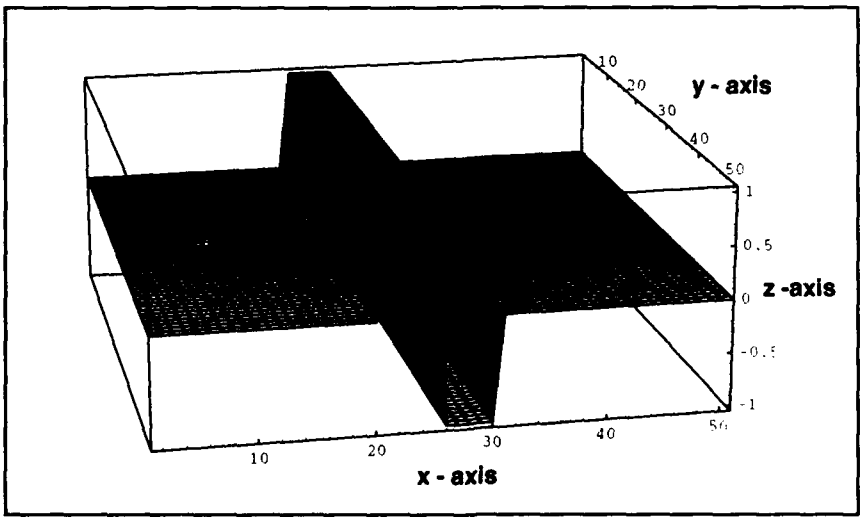

Figure 17. 1-D Haar wavelet required to highlight vertical edges

Fourier transform the function. This function can be considered the difference of two, one-dimensional rectangle functions. The first rectangle function would have a width of .5, be centered at $x = -.25$, and have a height of 1. The second rectangle function would have a width of .5, be centered at $x = .25$, and have a height of -1. Therefore, the Haar(x) function can be rewritten as:

$$\text{Haar}(x) \;=\; \text{rect}\left(\frac{x+.25}{.5}\right) \;-\; \text{rect}\left(\frac{x-.25}{.5}\right) \tag{17}$$

The Fourier transform of Haar(x) is obtained using this representation coupled with the following Fourier transform identity and property:

$$\begin{aligned} \mathcal{F}\left[\,\text{rect}(x)\,\right] &= \text{Sinc}(\xi), \\ \mathcal{F}\left[\,f\left(\frac{x-b}{a}\right)\,\right] &= |a|F(a\xi)e^{-j2\pi b\xi} \end{aligned} \tag{18}$$

The Fourier Transform of Haar(x) is:

$$\mathcal{F}\left[\,\text{Haar}(x)\,\right] \;=\; .5\text{Sinc}(.5\xi)e^{j2\pi(.25)\xi} \;-\; .5\text{Sinc}(.5\xi)e^{-j2\pi(.25)\xi} \tag{19}$$

This can be rewritten as:

$$\mathcal{F}\left[\,\text{Haar}(x)\,\right] \;=\; .5\text{Sinc}(.5\xi)\left(e^{j.5\pi\xi} \;-\; e^{-j.5\pi\xi}\right). \tag{20}$$

Using Euler's formula (8),

$$e^{j.5\pi\xi} \;-\; e^{-j.5\pi\xi} \;=\; (2j)\sin(.5\pi\xi).$$

Equation 20 is now given by:

$$\mathcal{F}\left[\,\text{Haar}(x)\,\right] \;=\; j\text{Sinc}(.5\xi)\sin(.5\pi\xi). \tag{21}$$

Since only the phase of the Fourier Transform is encoded in the CGH and we are only interested in phases that change as a function of the independent variable, ξ, we will ignore the constant phase factor of j. This yields:

$$\mathrm{Im}(\mathcal{F}\,[\,\mathrm{Haar}(x)\,]) \;=\; \mathrm{Sinc}(.5\xi)\sin(.5\pi\xi). \tag{22}$$

The absolute value of the two-dimensional Fourier Transform is shown in Figure 18 and its corresponding phase is shown in Figure 19. Since the Haar(x) wavelet is infinite in the y-dimension, it is expected that the Fourier Transform will collapse down onto the ξ-axis. This is exactly as shown in Figure 18.

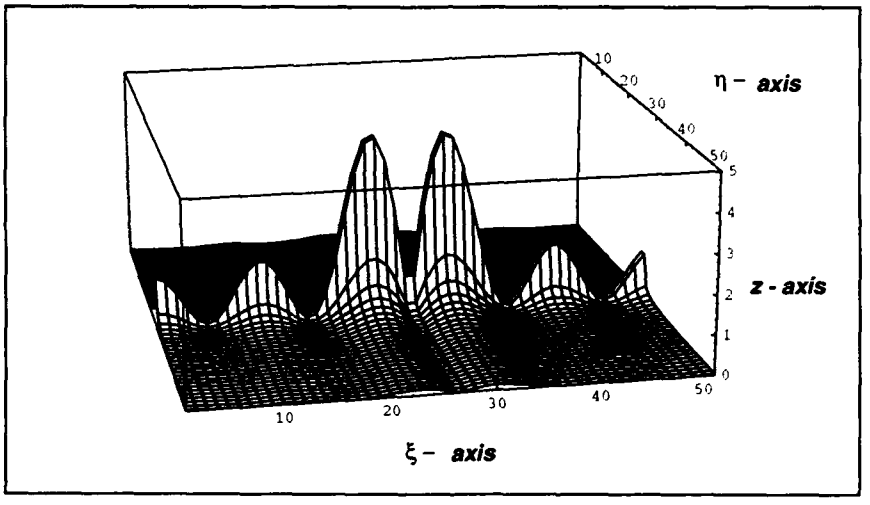

Figure 18. Absolute value of the Fourier Transform of 1-D Haar(x) wavelet

It is important to note that the phase of the Fourier Transform of a one-dimensional wavelet is independent of dilation. This means the phase function is constant for all of the dyadic dilations of the mother wavelet. Figures 20 and 21 are one-dimensional plots showing the amplitudes of the Fourier transforms of the one-dimensional wavelet for two different dilations. Both functions are positive or zero for positive values of ξ, and negative or zero for negative values of ξ. The phase of the magnitude of these two functions are identical except for the zero values

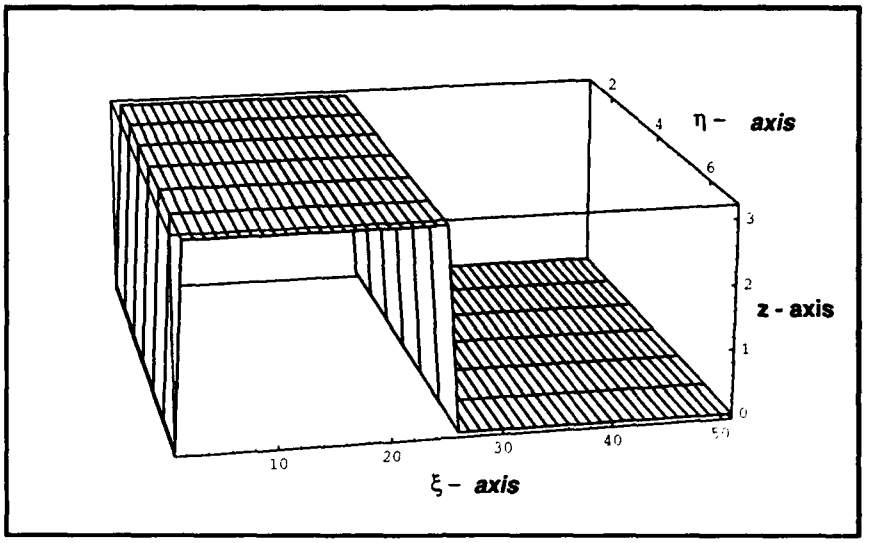

Figure 19. Phase of the Fourier Transform of 1-D Haar(x) wavelet

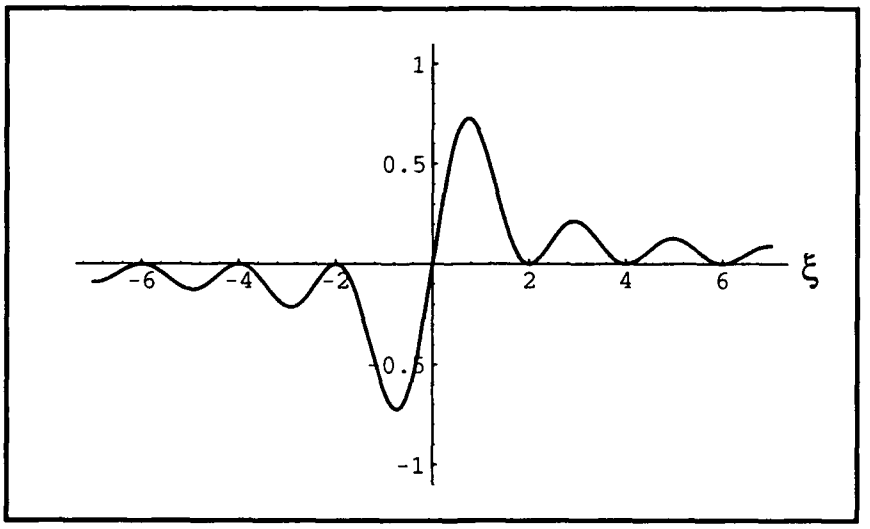

Figure 20. 1-D amplitude of the Fourier Transform of 1-D Haar(x) wavelet

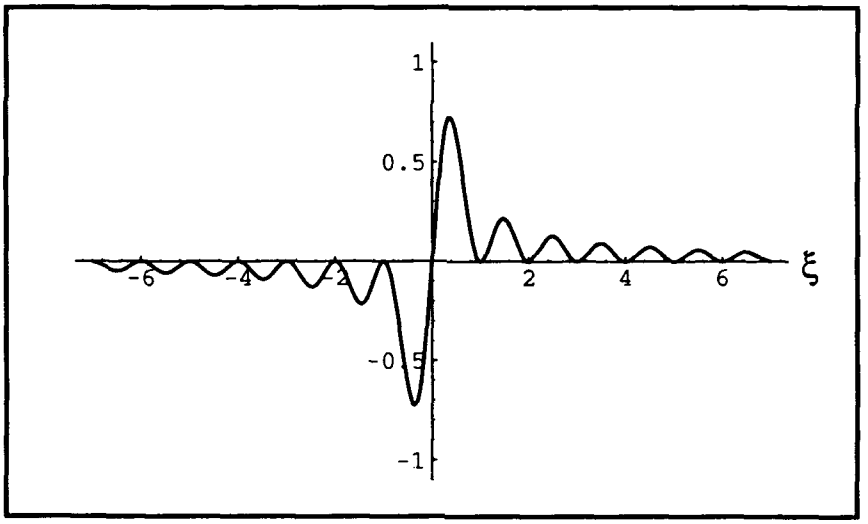

Figure 21. 1-D amplitude of the Fourier Transform of the first dyadic dilation of the 1-D Haar(x) wavelet

to the left of the origin. In order to have phase functions that differ for different dilations, it is necessary to make some assumptions. Figures 20 and 21 show that the amplitude of the Fourier transform drops off by more than a factor of three outside the first maxima. Therefore, we will assume the amplitude to be zero outside the first maxima as shown in Figures 22 and 23. Using this assumption, the phase function will change as the mother wavelet is scaled.

In order to predict how well the phase-only approximation of the Haar wavelet will perform in the correlator, it is necessary to inspect the Fourier transform of the CGH. The absolute value of the Fourier Transform of the CGH is shown in Figure 24. This function along with its first two dyadic dilations are encoded in CGHs.

The second one-dimensional wavelet function is Haar(y). This function will be used to filter horizontal spatial frequencies. The Haar(y) wavelet is identical to the Haar(x) wavelet except the x and y axes are interchanged. The expression for

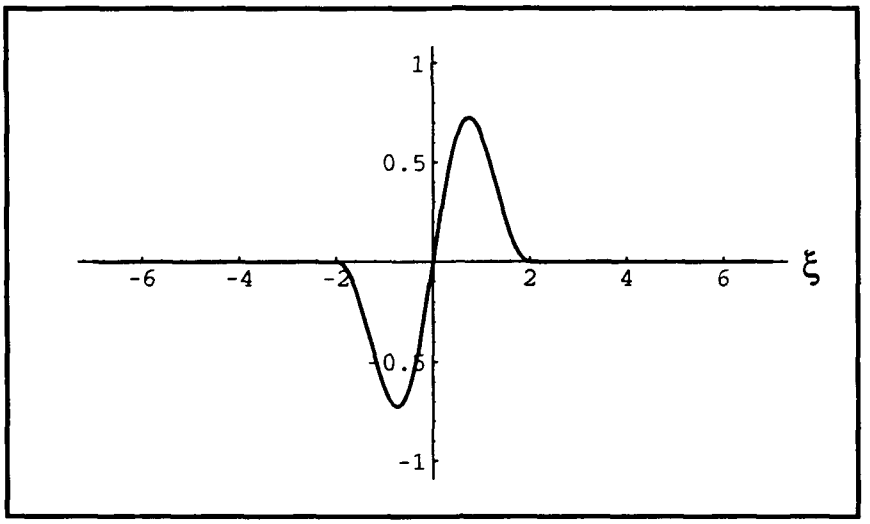

Figure 22. 1-D amplitude of the Fourier Transform of 1-D Haar(x) wavelet using assumption

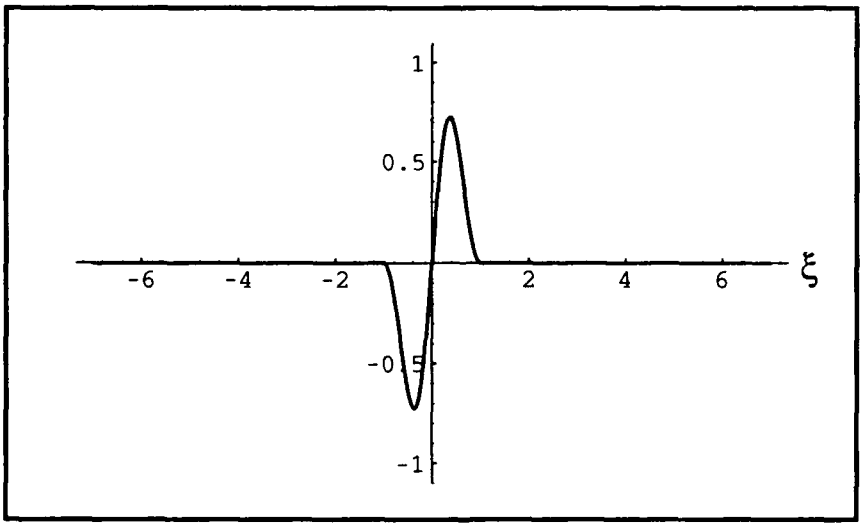

Figure 23. 1-D amplitude of the Fourier Transform of the first dyadic dilation of the 1-D Haar(x) wavelet using amplitude assumption

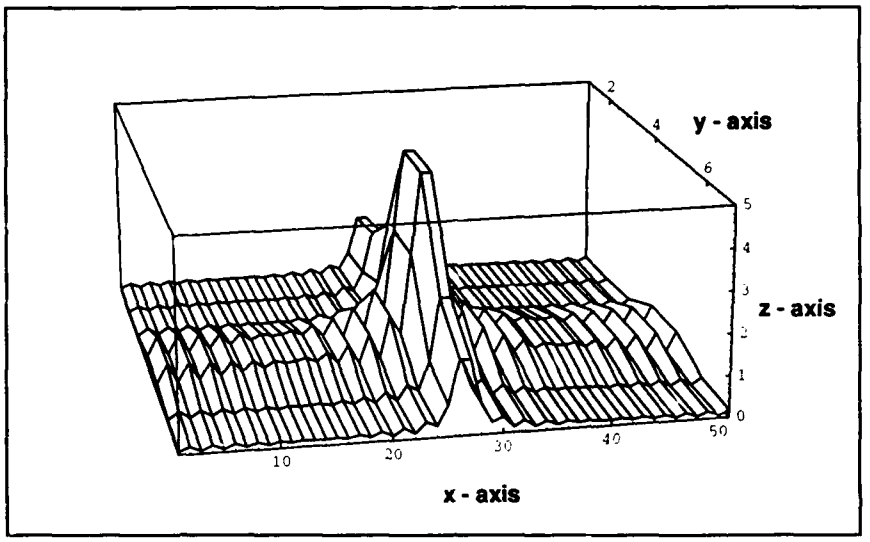

Figure 24. Absolute value of the Fourier Transform of the Phase of the Fourier Transform of 1-D vertical wavelet

Haar(y) is given below:

$$\text{Haar}(y) = \begin{cases} 1 & \text{if } -.5 \leq y < 0 \\ \text{-1} & \text{if } 0 \leq y < .5 \\ 0 & \text{otherwise} \end{cases} \tag{23}$$

The three-dimensional plots for the Haar(y) wavelet would be the same as the plot shown in Figures 17 - 19, but rotated counterclockwise by 90 degrees. Following the discussion presented in Equations 18-22, and substituting y for x and η for ξ yields:

$$\text{Im}(\mathcal{F}\,[\,\text{Haar}(y)\,]) \;=\; \text{Sinc}(.5\eta)\sin(.5\pi\eta). \tag{24}$$

The phase of this function along with its first two dyadic dilations are encoded in CGHs.

The last function to be encoded is the two-dimensional Haar(x,y) wavelet. The expression for the two-dimensional Haar(x,y) wavelet is given below:

$$\text{Haar}(x,y) = \begin{cases} 1 & \text{if } 0 \le x < .5 \text{ and } 0 \le y < .5 \;\; or \;\; -.5 \le x < 0 \text{ and } -.5 \le y < 0 \\ \text{-1} & \text{if } 0 \le x < .5 \text{ and } -.5 \le y < 0 \;\; or \;\; -.5 \le x < 0 \text{ and } 0 \le y < .5 \\ 0 & \text{otherwise} \end{cases} \quad (25)$$

This function can be written as the combination of four different rectangle functions as given by:

$$\begin{aligned} \text{Haar}(x,y) &= \text{rect}\left(\frac{x+.25}{.5}, \frac{y+.25}{.5}\right) + \text{rect}\left(\frac{x-.25}{.5}, \frac{y-.25}{.5}\right) \\ &- \text{rect}\left(\frac{x-.25}{.5}, \frac{y+.25}{.5}\right) - \text{rect}\left(\frac{x+.25}{.5}, \frac{y-.25}{.5}\right). \end{aligned} \quad (26)$$

The Fourier Transform of Haar(x,y) is obtained using the identities given in Equation 18 and yields:

$$\begin{aligned} \mathcal{F}\left[\text{ Haar}(x,y)\right] &= .25\text{Sinc}(.5\xi, .5\eta)\left[e^{-j2\pi(.25)(\xi+\eta)} + e^{j2\pi(.25)(\xi+\eta)}\right] \\ &- .25\text{Sinc}(.5\xi, .5\eta)\left[e^{j2\pi(.25)(\xi-\eta)} + e^{-j2\pi(.25)(\xi-\eta)}\right] \end{aligned} \quad (27)$$

Once again, ignoring the amplitude factor of .25 and applying Euler's formula yields:

$$\mathcal{F}\left[\text{ Haar}(x,y)\right] = \text{Sinc}(.5\xi, .5\eta)\ (\cos[.5\pi(\xi+\eta)] - \cos[.5\pi(\xi-\eta)]) \quad (28)$$

The phase of the function given in Equation 28 is shown in Figure 25. The negative spikes in Figure 25 correspond to zero values of the function over those intervals. In other words, the function is negative everywhere over those intervals except at those points where it is zero-valued. This function, along with its first two dyadic dilations

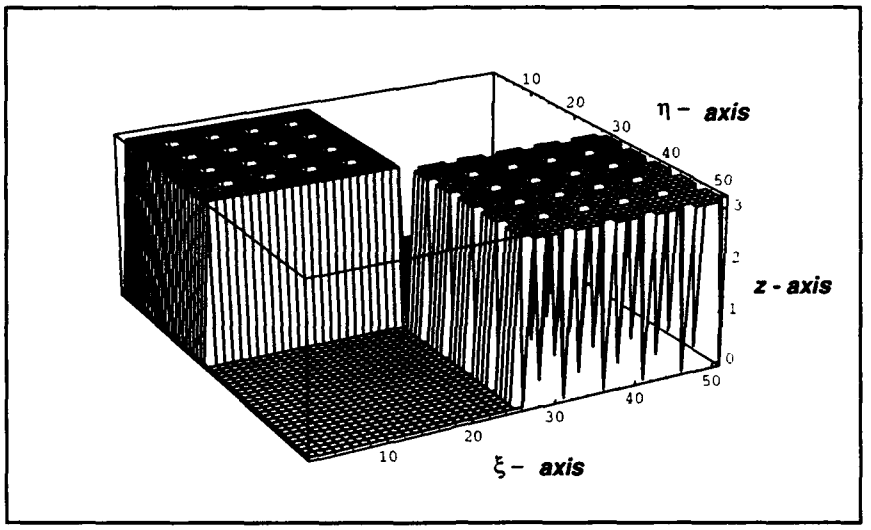

Figure 25. Phase of the Fourier Transform of 2-D Haar wavelet

are encoded in CGHs using the same assumption made for the one-dimensional wavelets.

4.4 Wavelet Transform Results

The input image used for the remainder of the research is shown in Figure 26. This image is used for this type of research because it has a wide variety of spatial frequencies within its image structure. A negative of this image was plotted on a 400 dot per inch laser printer, back illuminated using a Dekagon camera system (detailed in Appendix A) and then photoreduced onto a glass slide. This creates a positive image on the slide which is then placed in the input plane of the optical correlator system shown in Figure 7. Each CGH was then placed in plane, P2 and the correlation result was then captured using a CCD camera.

To validate the optical results, a series of digital simulations were performed. The digital simulations exactly modeled the optical system used. The optical results were then compared to the digital simulations to validate the results obtained. The next several pages provide the optical results of the wavelet transform along with its

Figure 26. Input image

corresponding digital simulation for ease of comparison. It should be noted that a slightly different version of the input image was used for all of the digital simulations. The digital simulation image is cropped slightly more than the image used in the optical system. The image used for the digital simulations is shown below.

The optical result obtained by using the unscaled mother wavelet, Haar(y), followed by its corresponding digital simulation are shown on the following page. The unscaled wavelet represents the narrowest passband filter and therefore is expected to pass the highest horizontal spatial frequencies. The vertical spatial frequencies are filtered out. Note that the pole on the left side of the image is not highlighted or filtered in Figures 28 and 29. In both figures, the edges of the hat, the eyebrows, as well as the shoulder are highlighted by the filter. The digital simulation compares very well to the optical result.

Figure 27. Digital simulation image

On the following page, the input image is filtered by the first dyadic dilation of the Haar(y) wavelet. The filter used in this correlation is coarser than that used on the previous page. This coarser filter will pass a wider band of spatial frequencies allowing more details of the image to be seen. This can be seen by looking at the hat feathers in Figures 30 and 31. More details of the feathers can be seen in Figures 30 and 31 than can be seen by looking at Figures 28 and 29. This is caused by the coarser filter used to obtain the results shown in Figures 30 and 31. Once again, the digital simulation compares very well to the optical result.

In Figures 32 and 33, the input image is filtered by the second dyadic dilation of the Haar(y) wavelet. The filter used in this correlation is coarser than that used for Figures 30 and 31. This filter passes an even wider band of spatial frequencies and therefore the results show even more details of the image. Note highlighting of the shoulder and the left side of the hat in both figures. The two figures compare favorably.

Figure 28. Optical result obtained using the Haar(y), unscaled, mother wavelet

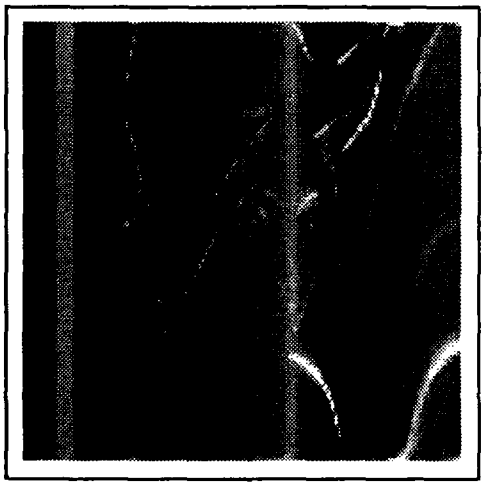

Figure 29. Digital simulation obtained using the Haar(y), unscaled, mother wavelet

Figure 30. Optical result obtained using the first dyadic scaling function and the Haar(y) mother wavelet

Figure 31. Digital simulation obtained using the first dyadic scaling function and the Haar(y) mother wavelet

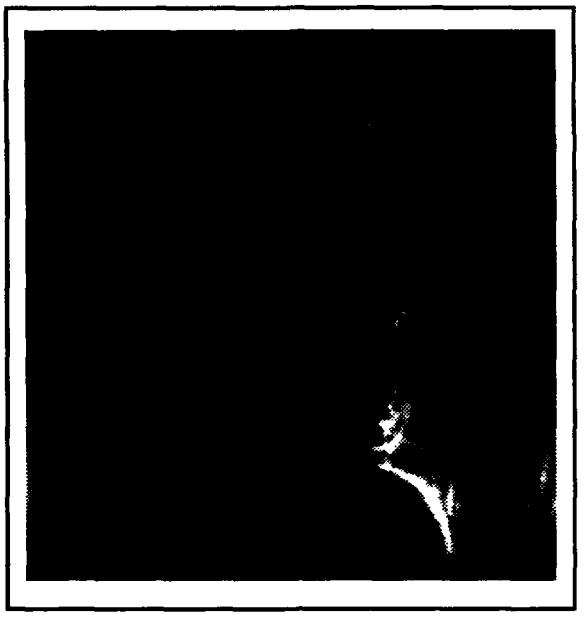

Figure 32. Optical result obtained using the second dyadic scaling function and the Haar(y) mother wavelet

Figure 33. Digital simulation obtained using the second dyadic scaling function and the Haar(y) mother wavelet

The optical result obtained by using the unscaled mother wavelet, Haar(x), followed by its corresponding digital simulation are shown on the following page. The unscaled wavelet represents the narrowest filter and therefore is expected to pass the highest vertical spatial frequencies. The horizontal spatial frequencies are filtered out. Note that the edges of the pole on the left side of the image are highlighted or filtered in Figures 34 and 35. In both Figures, the edges of the hat, the shoulder, as well as the right side of the face are highlighted by the filter. The digital simulation compares very well to the optical result.

On the next page, the input image is filtered by the first dyadic dilation of the Haar(x) wavelet. The filter used in this correlation is coarser than that used on the previous page. This coarser filter will pass a wider band of spatial frequencies allowing more details of the image to be seen. This can be seen by looking at the hat feathers in Figures 36 and 37. More details of the feathers can be seen in Figures 36 and 37 than can be seen by looking at Figures 34 and 35. This is caused by the coarser filter used to obtain the results shown in Figures 36 and 37. Once again, the digital simulation compares very well to the optical result.

In Figures 38 and 39, the input image is filtered by the second dyadic dilation of the Haar(x) wavelet. The filter used in this correlation is coarser than that used for Figures 36 and 37. This filter passes an even wider band of spatial frequencies and therefore the results show even more details of the image. Note slight highlighting of the shoulder and pole, as well as the hair on the right side of her face in both figures. The two figures compare favorably.

Figure 34. Optical result obtained using the Haar(x), unscaled, mother wavelet

Figure 35. Optical result obtained using the Haar(x), unscaled, mother wavelet

Figure 36. Optical result obtained using the first dyadic scaling function and the Haar(x) mother wavelet

Figure 37. Digital simulation obtained using the first dyadic scaling function and the Haar(x) mother wavelet

Figure 38. Optical result obtained using the second dyadic scaling function and the Haar(x) mother wavelet

Figure 39. Digital simulation obtained using the second dyadic scaling function and the Haar(x) mother wavelet

The optical result obtained by using the unscaled, two-dimensional mother wavelet, Haar(x,y), followed by its corresponding digital simulation are shown on the following page. This represents the last of the three wavelet basis functions. In both Figures, the edges of the hat, the shoulder, as well as the hair on the right side of the face are highlighted by the filter. The digital simulation compares well to the optical result.

On the next page, the input image is filtered by the first dyadic dilation of the Haar(x,y) wavelet. The filter used in this correlation is coarser than that used on the previous page. This coarser filter will pass a wider band of spatial frequencies allowing more details of the image to be seen. This can be seen by looking at the hat feathers in Figures 42 and 43. More details of the feathers can be seen in Figures 42 and 43 than can be seen in Figures 40 and 41. This is caused by the coarser filter used to obtain the results shown in Figures 42 and 43. Once again, the digital simulation compares very well to the optical result.

In Figures 44 and 45, the input image is filtered by the second dyadic dilation of the Haar(x,y) wavelet. The filter used in this correlation is coarser than that used for Figures 42 and 43. This filter passes an even wider band of spatial frequencies and therefore the results show even more details of the image. Note slight highlighting of the shoulder and pole, as well as the hair on the right side of her face in both figures. The two figures compare favorably.

Figure 40. Optical result obtained using the two-dimensional, unscaled, mother wavelet

Figure 41. Digital simulation obtained using the two-dimensional, unscaled, mother wavelet

Figure 42. Digital simulation obtained using the first dyadic scaling function and the two-dimensional mother wavelet

Figure 43. Digital simulation obtained using the first dyadic scaling function and the two-dimensional mother wavelet

Figure 44. Optical result obtained using the second dyadic scaling function and the two-dimensional mother wavelet

Figure 45. Digital simulation obtained using the second dyadic scaling function and the two-dimensional mother wavelet

Capturing the output correlations with the CCD camera varied with each CGH used. Each time a new CGH was placed in the optical correlation system, minor adjustments were made to the system alignment as well as the camera location. In all cases, the optical results compared favorably to the digital simulations.

4.5 Summary

This chapter introduced the wavelet analysis, multiresolution analysis, and the wavelet transform. The wavelet transform was used to filter an image. The optical results obtained with each wavelet and dilation were compared to its corresponding digital simulation. The digital simulations compared favorably to the optical results. The next chapter draws conclusions and makes recommendations to improve upon the results obtained. It also gives an overall summary of the research.

V. Conclusions and Recommendations

This research introduced an optical implementation of the continuous wavelet transform to filter images. The wavelet basis functions, required to perform the transform, were implemented with computer generated holography. This research had three main objectives. The first objective was to successfully filter images using the continuous wavelet transform. The second was to implement the continuous wavelet transform optically using computer generated holography. The last objective was to obtain better resolution than was obtained by Capt Pinski who used the Magneto-optic Spatial Light Modulator.

To validate the optical system and software used to encode the CGHs, an autocorrelation was performed using a known function. The results of the autocorrelation were compared to results obtained by digital simulation. The two results were identical. Next the continuous wavelet transform was introduced. The wavelet basis set was then defined and implemented with a CGH. The basis set consisted of two, one-dimensional Haar wavelets and the two-dimensional Haar wavelet. Each mother wavelet, along with its first two dyadic scalings, was implemented in the optical correlation system. The continuous wavelet transform performed a filtering operation on the input image. The results were captured with a CCD camera and provided in Chapter IV.

5.1 Conclusions

The continuous wavelet transform was implemented, using the Haar wavelet, in an optical correlator system. One assumption was required to encode different dilations of the Haar wavelet in the Interferogram CGH. The results compared favorably with the digital simulations except for the filtered images obtained using the dilated two-dimensional Haar wavelets. These images all contained some noise. It is not clear exactly what caused the noise in these images, however the close proximity

of the phase changes in those CGHs coupled with the quality of the CGH plot may have contributed to the less desirable results.

In each of the filtered images, too much detail of the input image is visible. If the results of the continuous wavelet transform will be passed to a neural network based system to segment the image, too much additional filtering is required. The Fourier transform of the Haar wavelet, as shown in Figures 20 and 21, varies greatly in amplitude as a function of the independent variable, ξ. Additionally, the phase of the Fourier transform of the Haar wavelet does not change as a function of dilation. Since the Interferogram CGH encodes only the phase of a function, it is not the best choice for encoding the Haar wavelet.

In addition, dark areas are visible in each of the filtered images. It is believed these dark areas are caused by the change in fringe line spacing occurring where the phase changes. To validate this hypothesis, the CGH of the first dyadic scaling function and the Haar(x) wavelet was bleached to lighten the fringe lines while maintaining the phase information. The bleached CGH allowed more light to pass through the system and improved the dark areas as can be seen by comparing the result shown in Figure 36 to the result shown in Figure 46 on the following page.

Lastly, this research was undertaken to improve the resolution of the results obtained by Pinski. Pinski's research used the Haar(x) and Haar(y) wavelets and implemented one dilation of each. His best results are shown on page 39 of his thesis (18). Comparison of his results with the results obtained in this research show improved resolution, however more detail of the image can also be seen. Additional processing would be required to remove the additional details present in the filtered images of this research.

5.2 Recommendations

Special assumptions were made to allow encoding of the dilated versions of the Haar wavelets. The assumption made to facilitate encoding of the Interferogram

Figure 46. Optical result obtained using the first dyadic scaling function and the Haar(x) mother wavelet with a bleached CGH

CGH can be eliminated if the phase as well as the amplitude information is encoded. This can be achieved using the detour-phase method of encoding CGHs. Because the detour-phase method will reduce the amount of light passing through the system, it is possible that a more powerful laser may be required. Since this method filters amplitude as well as phase, additional processing of the image discussed above would not be required. This system would more closely relate to that implemented by Pinski and allow for a better comparison of results.

Appendix A. *Creating a Computer Generated Hologram*

A.1 Introduction

Unlike regular photography where light from a scene is recorded on film in terms of its intensity(magnitude-squared), holography is a technique used to encode the magnitude and phase, or phase-only of the light originating from a three-dimensional object. This is usually done by optically interfering the light from an object with a reference beam and then recording the resulting interference pattern on a film plate (10). In many applications, it is necessary to create a hologram with a certain analytical magnitude and phase distribution. To do this, it is necessary to digitally calculate values of the magnitude and phase of the desired function for individual points. These data points can then be encoded into a real, nonnegative function which can be plotted using a standard laser printer. The plot, once photo-reduced onto a glass slide, is called a computer generated hologram.

This appendix provides the reader with all of the resources necessary to create phase-only computer generated holograms. First, the detailed background on the equations used to encode a computer generated hologram (CGH) is presented. Next, the software used to implement the derived equations is discussed in great detail. Lastly, the equipment used to photo-reduce the plotted transparency onto a glass slide is presented.

A.2 Encoding the CGH

The intensity variation resulting from an optically generated hologram is given by a transmittance function of the form

$$t(x,y) = R^2 + A^2(x,y) + 2RA(x,y)cos[2\pi\alpha x - \phi(x,y)]. \tag{29}$$

which is real and nonnegative(10). A(x,y) is the intensity (magnitude) of the light coming from the object and $\phi(x, y)$ is its phase. R is the intensity of the reference beam and α is the angle between the reference beam and the object beam. For the phase-only CGH, the transmittance function is given by(12):

$$t(x, y) = .5(1 + cos[2\pi\alpha x - \phi(x, y)]). \tag{30}$$

In this equation, α is the carrier frequency. The CGH will produce many diffracted waves when illuminated, therefore a sufficiently high carrier frequency must be chosen to separate the first diffracted order of the desired function from its higher orders(13). The transmittance functions above have maximums where the argument of the cosine term satisfies:

$$2\pi\alpha x - \phi(x, y) = 2\pi n_k, \tag{31}$$

for integer values of n_k, where k corresponds to a different fringe.

To test the theory, a two-dimensional rectangle function CGH was created. The rectangle function was chosen because its Fourier Transform is known and the phase of the Fourier Transform is discontinuous. For the two-dimensional rectangle CGH, $\phi(x, y)$ is a discrete function having a value of zero or pi depending on the sign of the Sinc function.

A.3 Plotting a CGH

The rectangle function was encoded and the CGH was plotted on a transparency using the C language software program provided in Appendix B. Although several commercial software packages are available to plot contour lines, or interference fringes, (including Matlab, Metalib, IDL, and Mathematica) none of them can handle functions containing sharp discontinuities as the phase functions shown in Chapters 3 and 4. The C program gave the best results. This work was accom-

plished on the Next Computers in the Signal Processing Lab, Room 2001, Building 642 at AFIT.

The C software program breaks up the plot into a 1600 by 1600 array of pixel values. Each pixel value maps to specific location in the two-dimensional spatial frequency plane. Since the output of the program is plotted on a transparency and then photoreduced onto a glass slide, the output plot must be a negative of the desired plot. In other words, if a single black line is required on a glass slide, the transparency must be opaque everywhere and clear where the line appears. The program loops through each pixel location, checks the sign of the Fourier Transform of the given function to determine the value of the phase function, ϕ, at that point. If the Fourier Transform is less than zero the phase is set to pi, otherwise the phase is set to zero. Next, the program evaluates the cosine function in Equation 31. Due to sampling considerations,the $2\pi\alpha x$ term in the argument of the cosine function was changed to $\frac{\pi}{2}x$. This ensures the cosine function will always be sampled at multiples of 90 degrees. If the cosine function is equal to one, the pixel is set to zero. Otherwise, the pixel is set to one. The loop continues until each pixel is assigned a value.

To compile and link all of the necessary files, a make file was created and is provided in Appendix E. The make file is run, using the terminal, simply by typing "make" followed by a carriage return. The program is run by typing the program name (in this case "petebin") followed by the name of the array the data is to be written to(in this case "templ"). After the program has run, the plot of the CGH is obtained by executing the make eps program provided in Appendix F. This program is run by typing "make_eps templ 1600 1600 6". In this command, templ is the name of the pixel array, 1600 is the size of the array in each direction, and 6 is the size of plot desired in inches.

A.4 Creating the CGH

Once the contour lines are plotted on a transparency, the transparency is taken to the Cooperative Electronics Materials Process Lab, room 1065 of building 125, to be reduced onto a high-resolution glass slide. A Dekagon Optical System was used to reduce the plot onto a glass slide and is shown in Figure 47.

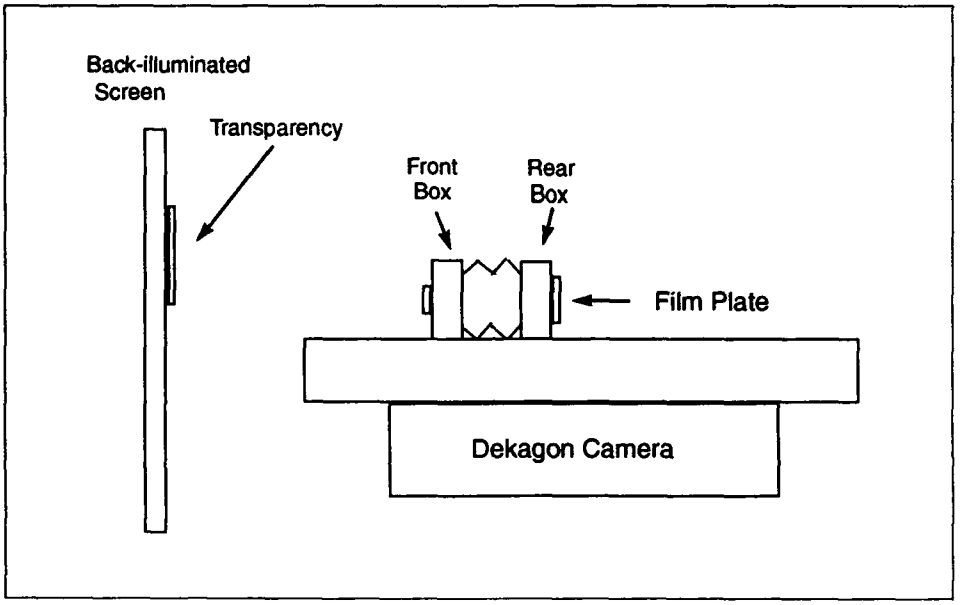

Figure 47. Dekagon Optical System

A 5 inch lens was placed on the front box and used to obtain a 20x reduction. This resulted in a CGH that was approximately 1.0cm by 1.0cm. To correctly align the system, the front and rear boxes were set at 49.97 and 70.05 respectively. These settings are only estimates of the correct alignment so the system must be focused. To do this, an exposed glass slide is scored with a sharp instrument on its emulsion side. The slide is then placed in the film plate with its emulsion side facing the screen and the transparency is place on the screen. Next, focus a microscope on the scored marks of the glass slide. After the marks are in focus, adjust the position of

the front box until both the contour lines and the score marks are in focus. Once this is done correctly, the Dekagon Optical System is correctly focused.

Next, in a darkroom, a 2in x 2in glass slide was placed in the film plate with the emulsion side facing down. The film plate was then mounted on the system. With the screen illuminated, the door closed, and the lights off, the shutter was removed and the slide was exposed for three minutes. The shutter was inserted back into the plate and then the plate was taken into the dark room for development. Once in the dark room, the slide was removed from the film plate and placed in a developer bath for two minutes. Next, the slide was placed in a fixer bath for two minutes. Finally, the slide was placed in the stop bath for two minutes, rinsed off in deionized water and then blown dry with nitrogen gas. To verify the system was focused properly, the slide was viewed under a microscope where clear, distinct lines were noted.

Please note the exposure time may vary based on how dark one wishes the lines to be and the age of the glass slides. The slides have expiration dates just like film and should be checked before using them. Also the amount of time the slides need to spend in the developer, fixer, and stop is a function of age and how many times each has been used previously. The times quoted in the previous paragraph were for freshly mixed chemicals.

A.5 Conclusions

Creating a CGH is a complex task. Use the software provided and your results should be excellent. It should be remembered however that nothing remains constant. Some of the steps highlighted in this report may require some fine adjustments. Remember, the measure of success is whether or not the CGH works on the optics bench.

Appendix B. *C Programs Used to Encode CGHs*

```
/*  This C program creates the matrix that defines the CGH of a  */
/*  two-dimensional rect function.                               */

#include <stdio.h>
#include <math.h>

float *vector();          /* Declare and initialize variables  */
float **matrix();

main(argc,argv)
int argc;
char **argv;

{int  x,y;
float *rdata;
float **pete;
double tmp,temp,phase,pi;
int number_points;
FILE *output_file;

number_points=1600;          /*  Define dimensions of CGH matrix  */

rdata=vector(1,number_points);

pete=matrix(1,number_points,1,number_points);
if (argc !=2)
{printf("need an output file");
exit(0);}
pi=3.141592654;
output_file = fopen(argv[1],"w");

for (y=1;y<=number_points;y++)   /* Initialize and start do while loops */
    {for (x=1;x<=number_points;x++)

/*  The next three nested if statements handle the discontinuities of */
/*  the Sinc function.                                                */
```

```
{if ((double)x/160.0-5.0== 0.0  & (double)y/160.0-5.0== 0.0)
{tmp=1.0;}

else if ((double)x/160.0-5.0== 0.0)
{tmp=sin(pi*((double)y/160.0-5.0))/(pi*((double)y/160.0-5.0));}

else if ((double)y/160.0-5.0== 0.0 )
{tmp=sin(pi*((double)x/160.0-5.0))/(pi*((double)x/160.0-5.0));}
else
 {tmp=sin(pi*((double)x/160.0-5.0))*sin(pi*((double)y/160.0-5.0))/
    (pi*pi*((double)x/160.0-5.0)*((double)y/160.0-5.0));}

if (tmp<0)     /* Check for phase of Sinc at current (x,y) value */
{phase=pi;}
else
{phase=0;}

temp=cos((double)((pi/2)*x - phase));

if (temp>=.9999999999)     /*  Check if at maxima of cosine  */
{pete[x][y]=0.0;}
else
{pete[x][y]=1.0;}

}  /*  end x loop */
}  /*  end y loop  */

printf("Values computed saving the data\n");
fflush(stdout);

for (y=1;y<=number_points;y++) /*  Write data to output file  */
{
for (x=1;x<=number_points;x++)
{rdata[x]=(float)pete[x][y];}
fwrite(rdata,sizeof(float),number_points,output_file);}

}  /*  end main  */

\newpage

/*  This C program creates the matrix that defines the CGH of a  */
/*  one-dimensional Haar wavelet.                                */
```

```
#include <stdio.h>
#include <math.h>

float *vector();          /* Declare and initialize variables  */
float **matrix();

main(argc,argv)
int argc;
char **argv;

{int  x,y;
float *rdata;
float **pete;
double tmp,temp,phase,pi;
int number_points;
FILE *output_file;

number_points=1600;          /*  Define dimensions of CGH matrix  */

rdata=vector(1,number_points);

pete=matrix(1,number_points,1,number_points);
if (argc !=2)
{printf("need an output file");
exit(0);}
pi=3.141592654;
output_file = fopen(argv[1],"w");

for (y=1;y<=number_points;y++)   /* Initialize and start do while loops */
    {for (x=1;x<=number_points;x++)


/*  The next two nested if statements handle the discontinuities of   */
/*  the Fourier Transform of the scaled Haar wavelet                   */

{if ((double)x/50.0-16.0== 0.0)
{tmp=0.0;}

else if (y> 600 & y<1000 & x>=0 & x<800)
{tmp=-1;}
else
```

```
      {tmp=1;}

if (tmp<0)     /* Check for phase of Haar at current (x,y) value */
{phase=pi;}
else
{phase=0;}

temp=cos((double)((pi/2)*x - phase));

if (temp>=.9999999999)     /*  Check if at maxima of cosine  */
{pete[x][y]=0.0;}
else
{pete[x][y]=1.0;}

}  /*  end x loop */
}  /*  end y loop  */

printf("Values computed saving the data\n");
fflush(stdout);

for (y=1;y<=number_points;y++) /*  Write data to output file  */
{
for (x=1;x<=number_points;x++)
{rdata[x]=(float)pete[x][y];}
fwrite(rdata,sizeof(float),number_points,output_file);}

}  /*  end main  */

\newpage

\newpage

/*  This C program creates the matrix that defines the CGH of a  */
/*  two-dimensional Haar wavelet.                                 */

#include <stdio.h>
#include <math.h>

float *vector();          /* Declare and initialize variables  */
float **matrix();

main(argc,argv)
```

```
int argc;
char **argv;

{int  x,y;
float *rdata;
float **pete;
double tmp,temp,phase,pi;
int number_points;
FILE *output_file;

number_points=1600;          /*  Define dimensions of CGH matrix  */

rdata=vector(1,number_points);

pete=matrix(1,number_points,1,number_points);
if (argc !=2)
{printf("need an output file");
exit(0);}
pi=3.141592654;
output_file = fopen(argv[1],"w");

for (y=1;y<=number_points;y++)   /* Initialize and start do while loops */
    {for (x=1;x<=number_points;x++)


/*  The next three nested if statements handle the discontinuities of */
/*  the Fourier Transform of the scaled 2-D Haar wavelet               */

{if ((double)x/160.0-5.0== 0.0  & (double)y/160.0-5.0== 0.0)
{tmp=0.0;}

else if ((double)x/160.0-5.0== 0.0)
{tmp=-1;}
else if ((double)y/160.0-5.0== 0.0 )
{tmp=-1;}
else if (y> 400 & y<1200 & x>=400 & x<1200)

{tmp=(cos(pi*((double)x/160.0-5.0+(double)y/160.0-5.0))-cos(pi*(((double)x/160.0-5.

else
{tmp=-1;}
```

```
if (tmp<0)     /* Check for phase of Haar at current (x,y) value */
{phase=pi;}
else
{phase=0;}

temp=cos((double)((pi/2)*x - phase));

if (temp>=.9999999999)     /*  Check if at maxima of cosine  */
{pete[x][y]=0.0;}
else
{pete[x][y]=1.0;}

}  /*  end x loop */
}  /*  end y loop  */

printf("Values computed saving the data\n");
fflush(stdout);

for (y=1;y<=number_points;y++) /*  Write data to output file  */
{
for (x=1;x<=number_points;x++)
{rdata[x]=(float)pete[x][y];}
fwrite(rdata,sizeof(float),number_points,output_file);}

}  /*  end main  */

\newpage

/*  This C program compiles the petebin program and links it     */
/*  with all required programs.                                  */

LIBS = -lNeXT_s -lsys_s   /usr/local/lib/libnr.a  -lm

all:  petebin flotbintogray

petebin: petebin.c
cc -g  -I/usr/local/include  -o petebin petebin.c $(LIBS)

flotbintogray: flotbintogray.c
cc -g  -I/usr/local/include  -o flotbintogray flotbintogray.c $(LIBS)

\newpage
```

```
/*  This is the make_eps software program used to convert the raw data  */
/*  to an eps format for plotting.                                      */

#!/bin/csh
if ($1 == "" || $2 == "" || $3 == "" || $4 == "") then
echo "  ";
echo "The proper format is:"
echo " "
echo "make_eps filename number_rows number_columns pictsize";
echo "  ";
exit -1
endif
set inputfile = $1

set temp = $1:r
echo $temp
flotbintogray $2 $3  $inputfile > $temp.gra
graytorle -o $temp.rle $3 $2 $temp.gra
rle2eps $temp $4
open $temp.eps

\newpage


/*  This software program is used by the make_eps software   */
/*  program.                                                 */

#include <stdio.h>
#include <math.h>
#include <string.h>
#include <stdlib.h>

float  **matrix();

main(argc,argv)
int argc;
char **argv;
{

/* command line:
flotogray row col infile > outfile
```

```
*/

  unsigned char       *rdata;
  int                 row,col, pixel, i, j;
  float **image;
  float max,min,threshold1,threshold2,temp;

  FILE *fp;

  if(argc!=4)
{
    fprintf(stderr,"flotogray: Syntax error!\n");
    fprintf(stderr, "Correct syntax: \n");
    fprintf(stderr,"flotogray row col   infile > outfile \n");
    exit(-1);
  }
        row = atoi(argv[1]);
col = atoi(argv[2]);

rdata=(unsigned char*)malloc(row*sizeof(unsigned char));
image = matrix(0,row-1,0,col-1);
fp = fopen( argv[3], "r");

for (i = 0; i < row; i++)
{for (j=0;j < col; j++)
{fread(&image[i][j],sizeof(float),1,fp);}
}
min = image[0][0];
for (i=0; i<row; i++)
{ for (j=0; j<col; j++)
  if ( image[i][j] < min ) min = image[i][j];
}
fprintf(stderr,"flotogray: min is %f\n", min);
for (i=0; i<row; i++)
{ for (j=0; j<col; j++)
  image[i][j]= image[i][j]-min;
}
max = image[0][0];

for (i=0; i<row; i++)
{ for (j=0; j<col; j++)
  if ( image[i][j] > max ) max = image[i][j];
```

```
}

fprintf(stderr,"flotogray : max is %f\n",max);

for (i=0; i<row; i++)
{ for (j=0; j<col; j++)
   image[i][j] = 255.0 - image[i][j]*255.0/max;
}

for (j=0; j<col; j++)
{
   for (i = 0; i<row;i++)
   {rdata[i]=(unsigned char)image[i][j];}
   fwrite(rdata,sizeof(unsigned char),row,stdout);
}

exit(0);
}
```

Bibliography

1. AT&T Electronic Photography and Imaging Center, Indianapolis,IN. *AT&T Truevision Advanced Raster Graphics Adapter TARGA 8 User's Guide* (Release 1.1 Edition), October 1985.
2. AT&T Electronic Photography and Imaging Center, Indianapolis,IN. *Truevision TARGA Demonstration Disk*, 1986.
3. AT&T Electronic Photography and Imaging Center, Indianapolis,IN. *Truevision TARGA Software Tools Notebook*(Release 4.0 Edition), August 1988.
4. Big Sky Software Corporation, Bozeman,MT. *Enhanced Beamcode Software*(Release 5.0 Edition), February 1988.
5. Bennett, Laura F. 'Knowledge-based evaluation of the segmentation component in automatic pattern recognition systems,' *Optical Enginering*, 30:154-164 (February 1991).
6. Burns, Thomas J. et al. 'Optical Haar wavelet transform,' *Optical Engineering*, 31:1852-1857 (September 1992).
7. Fielding, Capt Kenneth H. *A Position, Scale, and Rotation Invariant Holographic Associative Memory*. MS thesis, AFIT/GEO/ENG/88D-2. School of Engineering, Air Force Institute of Technology (AU), Wright-Patterson AFB OH, December 1988.
8. Gaskill, J. D. *Linear Systems, Fourier Transforms, and Optics*. New York: John Wiley and Sons, 1978.
9. Geiger, Davi and Alan Yuille. 'A Common Framework for Image Segmentation,' *International Journal of Computer Vision*, 6:227-243 (August 1991).
10. Goodman, J. W. *Introduction to Fourier Optics*. New York: McGraw-Hill Book Company, 1968.
11. Hecht, Eugene. *Optics* Reading, Mass.: Addison-Wesley Publishing Company, Inc., 1988.
12. Lee, Andrew J. *Optical Implementation/Realization of CT and LDF*. Appendix A to MS Thesis, School of Engineering, Carnegie-Mellon University, Pittsburgh PA, 1985.
13. Lee, Wai-Hon. 'Computer-Generated Holograms: Techniques and Applications,' *Progress in Optics*, 16:121-232 (1978)
14. Leseberg, Detlef. 'Computer-generated three-dimensional image holograms,' *Applied Optics*, 31:223-229 (January 1992).
15. Liou, Shih-Ping and Ramesh Jain. 'An Approach to Three-Dimensional Image Segmentation,' *Image Understanding*, 53:237-252 (May 1991).

16. Mallat, Stephane G. 'Multifrequency Channel Decomposition of Images and Wavelet Models,' *IEEE Transactions on Acoustics, Speech, and Signal Processing,* 37(12):2091-2110 (December 1989).

17. Mayo, 2Lt Michael W. *Computer Generated Hologram and Magneto-Optic Spatial Light Modulator for Optical Pattern Recognition.* MS thesis, AFIT/GEO/ENG/87D-1. School of Engineering, Air Force Institute of Technology (AU), Wright-Patterson AFB OH, December 1987.

18. Pinski, Capt Steven D. *Optical Image Segmentation Using Wavelet Correlation.* MS thesis, AFIT/GEO/ENG/91D-3. School of Engineering, Air Force Institute of Technology (AU), Wright-Patterson AFB OH, December 1991.

19. Rogers, Maj Steven K. 'Lecture Notes taken in EENG 620, Pattern Recognition I.' School of Engineering, Air Force Institute of Technology (AU), Wright-Patterson AFB OH, February 1992.

20. Smiley, Capt Steven E. *Image Segmentation Using Affine Wavelets.* MS thesis, AFIT/GE/ENG/91D. School of Engineering, Air Force Institute of Technology (AU), Wright-Patterson AFB OH, December 1991.

21. Tou, J. T. and R. C. Gonzalez. *Pattern Recognition Principles.* Reading, Mass.: Addison-Wesley Publishing Company, Inc., 1974.

22. Veronin, Christopher P. et al. 'Optical image segmentation using neural-based wavelet filtering techniques,' *Optical Engineering,* 31:287-294 (February 1992).

23. Wyrowski, Frank. 'Digital phase-encoded inverse filter for optical pattern recognition,' *Applied Optics,* 31:4650-4657 (November 1991).

Vita

Captain Peter G. Block was born on 4 April, 1963 in Neenah Wisconsin. He graduated from Rippowam High School in Stamford, Connecticut in 1981. He then attended the University of Connecticut where he was awarded a Bachelor of Science degree in Electrical Engineering. After graduation, he attended the Air Force Officer Training School where he was commissioned a second lieutenant on 21 August, 1985. His first assignment was with the Air Force Plant Representative Office (AFPRO) at Northrop Electronics Division in Hawthorne, California. While there, he served as the AFPRO Manager for the Peacekeeper ICBM Guidance System. In March of 1989, he was assigned to the Titan Expendable Launch Vehicles System Program Office at Los Angeles AFB, California. He served as the branch chief for electronic systems for the Titan II, Titan IV, and the Titan Centaur Upper Stage. He entered the School of Engineering, Air Force Institute of Technology in May 91.

Permanent address: 84 Skyview Drive
Southbury, Connecticut
06488

December 1992 Master's Thesis

OPTICAL HAAR WAVELET TRANSFORMS USING COMPUTER GENERATED HOLOGRAPHY

Peter G. Block

Air Force Institute of Technology, WPAFB OH 45433-6583

AFIT/GEO/ENG/92D-02

This research introduces an optical implementation of the continuous wavelet transform to filter images. The wavelet transform is modeled as a correlation process and is implemented with a Vander Lugt correlator. The orthonormal basis set used is composed of two one-dimensional Haar functions and a two-dimensional Haar function. Each wavelet, as well as its first two dyadic scalings, is implemented with computer generated holography. The Interferogram method, which represents a function only in terms of its phase, is used to encode the wavelet functions. The results are imaged onto a CCD array and captured using a framegrabber. The optical results are compared to digital simulation. The results show that an optical implementation of the continuous wavelet transform was performed and that the results compared favorably to digital simulation.

Wavelets, Holography, Optical Correlators 76

UNCLASSIFIED UNCLASSIFIED UNCLASSIFIED UL